Clim. Past Discuss., 8, 5493–5543, 2012
www.clim-past-discuss.net/8/5493/2012/
doi:10.5194/cpd-8-5493-2012

Climate of the Past Discussions

What controls the spatio-temporal distribution of D-excess and ^{17}O-excess in precipitation? A general circulation model study

C. Risi[1], A. Landais[2], R. Winkler[2], and F. Vimeux[2,3]

[1]Laboratoire de Météorologie Dynamique, UMR8539, CNRS, Institut Pierre Simon Laplace, Ecole Normale Supérieure (ENS), Ecole Polytechnique (EP), Université Pierre et Marie Curie (UPMC), UPMC Boite postale 99, 4 place Jussieu, 75752 Paris cedex 05, France
[2]Laboratoire des sciences du climat et de l'environnement (LSCE), UMR8212 (CEA-CNRS-UVSQ), CE Saclay, Orme des Merisiers, Bât. 701, 91191 Gif-sur-Yvette, Cedex, France
[3]Institut de Recherche pour le Développement (IRD), Laboratoire HydroSciences Montpellier (HSM), UMR5569 (CNRS-IRD-UM1-UM2), Montpellier, France

Received: 17 September 2012 – Accepted: 12 October 2012 – Published: 8 November 2012

Correspondence to: C. Risi (camille.risi@lmd.jussieu.fr)

Published by Copernicus Publications on behalf of the European Geosciences Union.

Abstract

Combined measurements of the $H_2^{18}O$ and HDO isotopic ratios in precipitation, leading to second-order parameter D-excess, have provided additional constraints on past climates compared to the $H_2^{18}O$ isotopic ratio alone. More recently, measurements of $H_2^{17}O$ have led to another second-order parameter: ^{17}O-excess. Recent studies suggest that ^{17}O-excess in polar ice may provide information on evaporative conditions at the moisture source. However, the processes controlling the spatio-temporal distribution of ^{17}O-excess are still far from being fully understood.

We use the isotopic general circulation model LMDZ to better understand what controls D-excess and ^{17}O-excess in precipitation at present-day (PD) and during the last glacial maximum (LGM). The simulation of D-excess and ^{17}O-excess is evaluated against measurements in meteoric water, water vapor and polar ice cores. A set of sensitivity tests and diagnostics are used to quantify the relative effects of evaporative conditions (sea surface temperature and relative humidity), Rayleigh distillation, precipitation re-evaporation and supersaturation during condensation at low temperature.

Simulations suggest that in the tropics convective processes and rain re-evaporation are important controls on D-excess and ^{17}O-excess. In higher latitudes, the effect of distillation, transport and mixing balance the effect of supersaturation. Since these terms are very large and near cancellation, results for both PD and LGM are very sensitive to the supersaturation function. The lower D-excess and ^{17}O-excess at LGM simulated at LGM are dominated by the supersaturation effect. Evaporative conditions had previously been suggested to be key controling factors of D-excess and ^{17}O-excess. In LMDZ, evaporative conditions are key in explaining the PD latitudinal and seasonal distributions, but play little role for ^{17}O-excess and for LGM variations. However, the LMDZ may underestimate this role. More generally, some shortcomings in the simulation of ^{17}O-excess by LMDZ suggest that GCMs are not yet the perfect tool to quantify with confidence all processes controlling ^{17}O-excess.

CPD
8, 5493–5543, 2012

1 Introduction

Water stable isotopic measurements in ice cores have long been used to reconstruct past climates. In particular, the $H_2^{18}O$ and HDO isotopic ratio (expressed respectively through δD and $\delta^{18}O$) in polar ice cores have long been used as a proxy of past polar temperature (Johnsen et al., 1972; Lorius et al., 1979; Jouzel, 2003). Combined measurements of $H_2^{18}O$ and HDO isotopic ratio in precipitation, leading to second-order parameter D-excess (d-excess = $\delta D - 8\delta^{18}O$, Dansgaard, 1964), have provided additional constraints on past climates compared to the $H_2^{18}O$ or HDO ratios alone. Its interpretation is however more complex. First interpreted as a tracer of relative humidity conditions at the moisture source (Jouzel et al., 1982), it has been later interpreted in terms of the temperature at the moisture source or of shifts in moisture origin (Stenni et al., 2001; Vimeux et al., 2002; Masson-Delmotte et al., 2005). It is also impacted by mixing along trajectories (Hendricks et al., 2000) and local temperature (Masson-Delmotte et al., 2008) and is very sensitive to a poorly-constrained empirical parameter determining the supersaturation in polar clouds (Jouzel and Merlivat, 1984).

More recently, measurements of $H_2^{17}O$ have led to the definition of another second-order parameter: $^{17}O\text{-excess} = \left(\ln(\delta^{17}O/1000+1) - 0.528 \cdot \ln(\delta^{18}O/1000+1)\right)$. Since magnitudes of ^{17}O-excess are very small, they are multiplied by 10^6 and expressed in permeg (Landais et al., 2008). Recent studies suggest that ^{17}O-excess may provide information on evaporative conditions at the source of moisture (Barkan and Luz, 2007; Landais et al., 2008; Risi et al., 2010c). Potentially, the combination of $\delta^{18}O$, d-excess and ^{17}O-excess may thus enable us to describe more comprehensively past climate changes, including local temperature, moisture origin and conditions at the moisture source. However, processes controlling ^{17}O-excess appear even more complex than those controlling d-excess. As d-excess, ^{17}O-excess is strongly sensitive to the empirical parameter determining the supersaturation in polar clouds (Winkler et al., 2012b; Landais et al., 2012a,b). In addition, its logarithmic definition makes it very sensitive to

CPD
8, 5493–5543, 2012

mixing (Risi et al., 2010c). In Central Antarctica it may also be affected by less conventional processes such as stratospheric intrusions (Winkler et al., 2012a).

This paper aims at better understanding what processes controls the spatio-temporal distribution of d-excess and ^{17}O-excess, and what processes make δ^{18}O, d-excess and ^{17}O-excess complementary tracers. These questions have so far been addressed using simple models: Rayleigh distillation models (Landais et al., 2008, 2012b; Risi et al., 2010c) which can be coupled to a back-trajectory analysis (Winkler et al., 2012b), a single column model (Risi et al., 2010c) or a bulk re-evaporation model (Landais et al., 2010). To take into account a broader range of processes controlling the water isotopic composition, we use the isotope-enabled general circulation model (GCM) LMDZ (Risi et al., 2010b), in which we have implemented $H_2^{17}O$. The added value of GCMs compared to simpler models is that they represent the integrated effect along air mass trajectories of boundary layer and convective processes, cloud and precipitation physics, evaporative recycling and mixing between different air masses. To investigate the effect of this combination of processes, isotopic GCMs are irreplaceable. For example, isotopic GCM simulations have been exploited to understand how δ^{18}O and d-excess relate to the origin of water vapor (e.g. Delaygue, 2000; Werner et al., 2001; Noone, 2008; Lee et al., 2008; Masson-Delmotte et al., 2011). The drawback of a GCM is however its difficulty to simulate some aspects of observed d-excess variability (e.g. Werner et al., 2001; Noone, 2008). This difficulty reflects the complexity of the d-excess parameter and our lack of understanding of its major controlling factors. This difficulty is expected to be even more severe for ^{17}O-excess.

To our knowledge, this is the first time ^{17}O-excess simulations with a GCM are being documented. The first goal of this paper is thus to document the performance of GCMs in capturing observed spatio-temporal variations in ^{17}O-excess. This allows us to better assess the feasibility of using a GCM to investigate what controls ^{17}O-excess. For features that the model can capture well, we use the GCM to disentangle the different processes controlling ^{17}O-excess and contrast them with processes controlling δ^{18}O and d-excess. For features that the model cannot capture well, we suggest possible

CPD
8, 5493–5543, 2012

causes of mismatches. As a first study of ^{17}O-excess in a GCM, we focus on latitudinal gradients, seasonal variability and difference between the Last Glacial Maximum (LGM) and present-day (PD).

In Sect. 2, we describe the model simulations, the datasets used for its validation and the methodology used to quantify the factors controlling the isotopic distributions. In Sect. 3, we evaluate the model isotopic simulations for both PD and LGM. In Sect. 4, we quantify the factors controlling the δ^{18}O, d-excess and ^{17}O-excess distributions simulated by LMDZ. Based on the strengths and weaknesses of LMDZ highlighted in Sect. 3, we discuss implications for what controls isotopic distributions in the real world. In Sect. 5, we summarize our result and present perspectives for future work.

2 Model simulations, datasets and methodology

2.1 The LMDZ4 model and isotopic implementation

LMDZ4 (Hourdin et al., 2006) is the atmospheric component of the Institut Pierre-Simon Laplace coupled model (IPSL-CM4, Marti et al., 2005) used in CMIP3 (Coupled Model Intercomparison Project, Meehl et al., 2007). It is used here with a resolution of 2.5° in latitude, 3.75° in longitude and 19 vertical levels. The physical package includes the Emanuel convective scheme (Emanuel, 1991; Emanuel and Zivkovic-Rothman, 1999) and a statistical cloud scheme (Bony and Emanuel, 2001). Water vapor and condensate are advected using a second order monotonic finite volume advection scheme (Van Leer, 1977; Hourdin and Armengaud, 1999).

The isotopic version of LMDZ is described in detail in Risi et al. (2010b). Equilibrium fractionation coefficients between vapor and liquid water or ice are calculated after Merlivat and Nief (1967), Majoube (1971a) and Majoube (1971b). The isotopic composition of the ocean surface evaporation flux is calculated following Craig and Gordon (1965). We take into account kinetic effects during the evaporation from the sea surface following Merlivat and Jouzel (1979) and during snow formation following Jouzel and

CPD
8, 5493–5543, 2012

Merlivat (1984), with the supersaturation parameter λ set to 0.004 to optimize the simulation of d-excess over Antarctica (Risi et al., 2010b). This λ value is consistent with that found to optimize the simulation of both d-excess and ^{17}O-excess in both Antarctica and Greenland in simpler models (Landais et al., 2012a,b). We assume that over land, all evapo-transpiration occurs as non-fractionating transpiration. Specifically for $H_2^{17}O$, equilibrium fractionation coefficient are equal those for $H_2^{18}O$ at the power 0.529 (Van Hook, 1968; Barkan and Luz, 2005; Landais et al., 2012b). The diffusivity of $H_2^{17}O$ relatively to that of $H_2^{16}O$ is assumed to be that for $H_2^{18}O$ at the power 0.518 (Barkan and Luz, 2007).

We do not consider the effect of methane oxydation on the stratospheric water isotopic composition (Johnson et al., 2001; Zahn et al., 2006). This is a reasonable approximation since we focus on the isotopic composition of the precipitation and low-level vapor. It has been shown that in Central Antarctica, stratospheric intrusions may play a role in the inter-annual variability of Vostok precipitation ^{17}O-excess, but the role of these intrusions in the spatial and seasonal distribution of ^{17}O-excess and in its LGM-to-present variation is unclear.

The implementation of stable water isotopes in the convective scheme has been extensively described in Bony et al. (2008). We pay particular attention to the representation of the re-evaporation and diffusive exchanges as the rain falls, which is significantly different compared to other GCMs. The relative proportion of evaporative enrichment and diffusive equilibration is calculated depending on surrounding relative humidity following Stewart (1975). The surrounding relative humidity is calculated as $\phi + (1-\phi)\cdot h_{\mathrm{ddft}}$ with h_{ddft} the relative humidity in the unsaturated downdrafts that collect the precipitation. The parameter ϕ was set to 0.9 to optimize the simulation of δ^{18}O and d-excess in tropical rainfall and their relationship with precipitation rate (Risi et al., 2010b), although $\phi = 0.8$ is in better agreement with some ^{17}O-excess data (Landais et al., 2010). The model takes into account the evolution of the compositions of both the rain and the surrounding vapor as the rain drops reevaporate (Bony et al., 2008). When the relative humidity is 100 % we simply assume total reequilibration between

CPD
8, 5493–5543, 2012

raindrops and vapor, contrary to Stewart (1975) and Lee and Fung (2008) who take into account the raindrop size distribution in this particular case.

Our calculation of isotopic exchanges during rain re-evaporation involves in the general case the numerical solution of an integral (Bony et al., 2008). The number of iterations used in this solution was chosen to be sufficient to accurately predict $\delta^{18}O$ and d-excess, but was found to be insufficient to predict ^{17}O-excess. The number of iterations was thus multiplied by 2, which makes the simulation with $H_2^{17}O$ computationally slower than usual.

2.2 Model simulations

Due to computational limitations, all simulations are short (2–3 yr) but use as initial states outputs of simulations that have already been equilibrated for several years for all isotopes.

To compare with datasets, LMDZ is forced by observed sea surface temperatures (SST) and sea ice following the AMIP (Atmospheric Model Inter-comparison Project) protocol (Gates, 1992) for the year 2005–2006. The year 2005–2006 was chosen to allow daily collocation with the vapor dataset of Uemura et al. (2010). Horizontal winds at each vertical level are nudged by ECMWF reanalyses (Uppala et al., 2005) as detailed in Risi et al. (2010b). This ensures a realistic large-scale circulation. When comparing with the other datasets, some of the model-data difference could be attributed to the differences in the meteorological conditions between 2005–2006 and the year of the measurement. Ideally, the full period 2000–2010 should have been simulated and outputs should have been collocated with each measurement for a perfectly rigorous comparison. However, for the first GCM evaluation for ^{17}O-excess, we focus on broad latitudinal gradients and seasonal variations that are robust with respect to inter-annual variability.

To investigate controls at paleo-time scales, we focus on the LGM period for which a large number of paleo-climate proxies are available (e.g. Farrera et al., 1999; Bartlein et al., 2010) and the forcing is relatively well-known (Braconnot et al., 2007) and strong.

CPD
8, 5493–5543, 2012

For the PD control simulation, LMDZ is run without nudging and forced by climatological AMIP SSTs averaged over 1979–2007. For the LGM simulation, the PMIP1 protocol is applied (Joussaume and Taylor, 1995). LMDZ is forced by SSTs and sea-ice from the LongRange Investigation, Mapping, and Prediction (CLIMAP, CLIMAP, 1981) forcing. Orbital parameters and greenhouse gas concentrations are also set to their LGM values. ICE-5G ice-sheet conditions are applied (Peltier, 1994). This simulation is described in Risi et al. (2010b). We use CLIMAP rather than the SSTs simulated by a coupled model (as in the PMIP2 protocol, Braconnot et al., 2007), because the SSTs and sea-ice simulated by the IPSL model at LGM are unrealistically warm in the Southern Ocean (Risi et al., 2010b). We are aware of the caveats of the CLIMAP forcing. In particular, the warm tropical SSTs and the extensive sea ice of the CLIMAP reconstruction have been questioned (MARGO project members, 2009). However, since our LGM evaluation will focus on Antarctica where most of the ^{17}O-excess so far have been available for LGM, we prefer the caveats of CLIMAP than those of the IPSL model.

2.3 Datasets for model evaluation

To evaluate the present-day nudged simulation of δ^{18}O and d-excess, we use the GNIP (Global Network of Isotopes in Precipitation) dataset (Rozanski et al., 1993) as is done in all basic isotopic modelling publications (Hoffmann et al., 1998; Risi et al., 2010b). This dataset was complemented with Antarctica (Masson-Delmotte et al., 2008) and Greenland (V. Masson-Delmotte, personal communication, 2008) data and was regridded on the LMDZ grid.

For ^{17}O-excess, we use a set of meteoric water measurements compiled by Luz and Barkan (2010). This includes measurements in precipitation, snow, rivers and lakes (Table 1). When comparing LMDZ with observed composition in the precipitation, we collocate with the month of the sampling for precipitation. When comparing LMDZ with observed composition in river water, we calculate annual-mean precipitation composition, because we assume that river water is representative of the annual-mean precipitation (Kendall and Coplen, 2001). We add to this set some ^{17}O-excess

CPD
8, 5493–5543, 2012

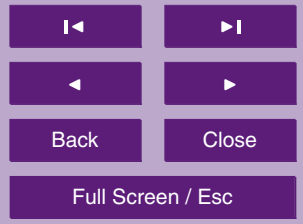

measurements made at LSCE (Table 2): monthly-mean precipitation in the Zongo Valley in Bolivia (Vimeux et al., 2005, unpublished for d-excess and ^{17}O-excess), in Niamey (Niger, Landais et al., 2010), in NEEM (Greenland, Landais et al., 2012b) and in Vostok (Antarctica, Winkler et al., 2012b). We also add δ^{18}O, d-excess and ^{17}O-excess measurements along an Antarctica transect (Landais et al., 2008). To evaluate the composition of the water vapor, we use the δ^{18}O, d-excess and ^{17}O-excess measurements made during Southern Ocean cruises in 2005–2006 (Uemura et al., 2008, 2010). Finally, we use the isotopic composition measured from PD to LGM in several Antarctica ice cores: Vostok (Landais et al., 2008), Taylor Dome and Dome C (Winkler et al., 2012b) (Table 3). The precision of these measurements is about 5 permeg (Landais et al., 2006).

There are calibration issues affecting absolute measurements of ^{17}O-excess (Winkler et al., 2012b; Landais et al., 2012a). In particular, there are ^{17}O-excess calibration uncertainties for large δ^{18}O variations. This effect leads to an uncertainty of 20 permeg for δ^{18}O variations of 50 ‰. Such an uncertainty is beyond measurement precision for δ^{18}O variations larger than 12.5 ‰. Therefore, there is some uncertainty in the latitudinal variations of ^{17}O-excess through Antarctica, where δ^{18}O strongly varies. However, other spatial patterns as well as seasonal and LGM-PD variations, which are characterized by smaller δ^{18}O variations, are not affected by this problem and can thus be considered robust.

2.4 Methodology to quantify isotopic controls

Precipitation δ^{18}O, d-excess and ^{17}O-excess are decomposed into several contributions. For simplicity, we present here the method for decomposing the isotopic ratio R for any of the 3 heavy isotopic species (HDO, $H_2^{18}O$, $H_2^{17}O$), but the same equations apply for δ^{18}O, d-excess and ^{17}O-excess.

Precipitation composition is first decomposed into 2 terms:

$$R_p = R_v + \left(R_p - R_v\right)$$

CPD
8, 5493–5543, 2012

The first term R_v is the vapor composition. It results from all processes affecting the isotopic composition of the vapor upstream air mass trajectories. The second term is the precipitation-vapor difference. This reflects local condensation and post-condensation processes, since precipitation is produced and falls locally. In the tropics, where the precipitation is liquid, $R_p - R_v$ will mainly reflect rain re-evaporation. At high latitudes, where precipitation is solid and is thus not affected by post-condensational processes, $R_p - R_v$ will depend on the condensation altitude, temperature and rate. It can also depend on the vertical gradient of water vapor isotopic composition between the surface and the condensation altitude.

Then, several sensitivity tests are used to understand what controls the vapor composition. Since ^{17}O-excess has been shown to be affected by evaporative conditions at the moisture source and to be sensitive to kinetic fractionation during ice-condensation, we quantify preferentially these two kinds of effects. To quantify the effect of evaporative conditions, we make additional simulations in which the sea surface temperature (SST) or the relative humidity normalized by the surface temperature (rh_s) during the calculation of isotopic fractionation at ocean evaporation are fixed constant. This allows us to quantify the direct effect of SST and rh_s at the moisture source without changing anything in the dynamics or in the hydrological cycle of the simulation. We call RH_scste the simulation in which the rh_s is set to 60 % during the calculation of isotopic fractionation at ocean evaporation. The effect of rh_s at the source is thus $\Delta R_{RH_s} = R_{v,control} - R_{v,RH_s cste}$. We call RH_sSSTcste the simulation in which the SST is set to 15 °C and the rh_s is set to 60 % during the calculation of isotopic fractionation at ocean evaporation. The effect of SST at the source is thus $\Delta R_{SST} = R_{v,RH_s cste} - R_{v,RH_s SSTcste}$.

To quantify kinetic fractionation during ice-condensation, we perform an additional simulation (called nokin) in which this fractionation is turned off, i.e. λ is set to 0. The effect of kinetic fractionation during ice condensation is thus $\Delta R_{kin} = R_{v,control} - R_{v,nokin}$.

CPD
8, 5493–5543, 2012

Assuming that all processes add up linearly, we can thus decompose R_v into four terms:

$$R_{v,control} = \left(R_{v,RH_sSSTcste} - \Delta R_{kin}\right) + \Delta R_{kin} + \Delta R_{SST} + \Delta R_{RH_s} \quad (1)$$

The first term on the right hand side represents all the processes other than evaporative conditions and kinetic fractionation during ice condensation. In the tropics, this may represent for example convective mixing by unsaturated downdrafts (Risi et al., 2008a, more details in Sect. 4.3.1). In higher latitudes, this represents Rayleigh distillation along trajectories, transport processes and mixing between different air masses.

3 Model evaluation

We first evaluate the simulation of the triple isotopic composition in the water vapor, and then in the precipitation.

3.1 Water vapor isotopic composition

Few observations are available for ^{17}O-excess in the water vapor. We compare LMDZ with water vapor isotopic composition measured in the near surface vapor along Southern Ocean transects (Uemura et al., 2008, 2010). When going poleward, observed $\delta^{18}O$ decreases consistently with the distillation of air masses (Fig. 1a, red). At the same time, d-excess and ^{17}O-excess decrease (Fig. 1b, c). This is consistent with the effect of evaporative conditions on d-excess and ^{17}O-excess (Vimeux et al., 2001a; Landais et al., 2008; Risi et al., 2010c). The rh_s increases poleward (Fig. 1d) while the SST decreases. Both rh_s and SST effects contribute to the poleward decrease of d-excess and ^{17}O-excess (Appendix A).

The Merlivat and Jouzel (1979) closure equation (Appendix A) captures the poleward decrease in d-excess and ^{17}O-excess (Fig. 1, dashed green). This can be visualized in a synthetic way by plots of d-excess and ^{17}O-excess as a function of rh_s (Fig. 1e,

CPD
8, 5493–5543, 2012

f). Corresponding slopes are shown in Table 4. According to the Merlivat and Jouzel (1979) closure, 73 % of the d-excess decrease as a function of rh_s is due to the direct effect of rh_s, and the remaining is due to the effect of SST. Virtually all of the ^{17}O-excess decrease as a function of rh_s is due to the direct effect of rh_s. This is because SST has a very small effect on ^{17}O-excess due to its log definition (Landais et al., 2008). We notice that the Merlivat and Jouzel (1979) closure predicts a larger ^{17}O-excess-vs-rh_s slope than observed. This suggests that some processes, such as boundary layer mixing with the free troposphere, act to dampen the ^{17}O-excess sensitivity to evaporative conditions.

The water vapor composition at the lowest model level simulated by LMDZ is compared to the data for each measurement day and location. LMDZ captures the rh_s distribution as a function of latitude well, with an increase in rh_s with latitude (Fig. 1a, blue). It also simulates the poleward decrease in δ^{18}O, d-excess and ^{17}O-excess. However, it overestimates the poleward decrease in δ^{18}O (by about 60 % from 35° S to 67° S) and underestimates the poleward decrease in d-excess (by about 65 %) and ^{17}O-excess (by about 70 %). As a result, the slopes of the rh_s-d-excess and rh_s-^{17}O-excess relationships are underestimated, by about 65 % and 70 % respectively (Fig. 1e, f, Table 4). The lack of sensitivity of d-excess to rh_s in LMDZ was already noticed when comparing to water vapor measurements in Greenland (Steen-Larsen et al., 2012).

This lack of sensitivity could be due to several kinds of problems. First, there could be problems in the composition of the evaporation flux. The prediction by the Craig and Gordon (1965) equation used in LMDZ may not be adequate. However, this does not appear to be the case, since the Merlivat and Jouzel (1979) closure approximation, which applies the same Craig and Gordon (1965) equation, is in good agreement with the observations (Fig. 1e, f). Using the LMDZ simulations RH_sSSTcste and RH_scste, we estimate that LMDZ underestimates the rh_s and SST effects in similar proportions: 37 % and 31 % respectively (Table 4). This suggests that in LMDZ, the sensitivity to SST and to rh_s are dampened by some atmospheric processes that are unrelated to evaporative conditions.

CPD
8, 5493–5543, 2012

Second, there could be some altitude mismatch between the near-surface vapor collected on the ship (a few meters), and the vapor of the first layer of the model (0–130 m). This hypothesis is supported by the fact that the simulated $\delta^{18}O$ latitudinal gradient in the low-level vapor is steeper than in that observed in the near-surface vapor (Fig. 1a). As a simple interpolation, we calculate near-surface vapor $\delta^{18}O$ as a mixture between the low-level vapor and the evaporation flux. When doing so, the $\delta^{18}O$ latitudinal gradient becomes less steep (Fig. 1a, cyan). Quantitatively, adding 7 % of surface evaporation appears optimal to match the observed variations in near-surface $\delta^{18}O$. However, adding 7 % of evaporation flux has little influence on d-excess and ^{17}O-excess (Fig. 1b, c, cyan). Therefore, the altitude mismatch is unlikely to explain the d-excess and ^{17}O-excess mismatch.

Third, there could be problems in the boundary layer parameterization. If the boundary layer mixing is too strong, then the evaporative signal in the near-surface vapor may be dampened by advection of free-tropospheric air. To test this hyothesis, the mixing length scale used in the boundary layer parameterization is halved (Fig. 1 purple). However, this does little to improve d-excess and ^{17}O-excess.

Fourth, there could be all kinds of other problems affecting the free-tropospheric vapor entrained into the boundary layer. In particular, some processes in the subtropics that lower the tropospheric d-excess and ^{17}O-excess could be over-simulated in the model (e.g. liquid condensation for d-excess, mixing for ^{17}O-excess), and other processes that increase the tropospheric d-excess and ^{17}O-excess could be under-simulated (e.g. rain drop re-evaporation). The range of processes that could be misrepresentated is very large and the sensitivity tests that we have done so far have not allowed us to identify the culprit yet. When interpreting the results in Sect. 4, we just need to remember that the effect of evaporative conditions will be likely underestimated.

CPD
8, 5493–5543, 2012

3.2 Spatial distribution

The simulated spatial patterns of annual mean $\delta^{18}O$, d-excess and ^{17}O-excess are compared with observations in Fig. 2. The latitudinal gradients are summarized in Fig. 3. In the latter figure, model outputs and observations are collocated for a more quantitative comparison.

The simulated annual mean spatial and zonal distribution of $\delta^{18}O$ and d-excess were already extensively evaluated in Risi et al. (2010b). Spatial patterns of $\delta^{18}O$ are very well captured, including the main "effects" that have long been documented (Dansgaard, 1964; Rozanski et al., 1993): latitudinal gradient associated with the temperature effect, the land-sea contrast with more depleted values over land associated with the continental effect, and the depletion of the South Asia–Western Pacific region, associated with the amount effect. The root mean square error of simulated $\delta^{18}O$ is 3.5 ‰ globally. The latitudinal gradient in polar regions is underestimated, due to the warm bias in these regions (Risi et al., 2010b).

Spatial patterns for d-excess are also relatively well captured: a minimum in the Southern Ocean and over the coasts of Antarctica, a minimum over North-Western America and Alaska, a minimum over the Sahel region (associated with rain re-evaporation, Risi et al., 2008b) and a maximum over the Mediteranean and Middle-East region (interpreted as the effect of strong kinetic fractionation during sea surface evaporation in a dry environment, Gat et al., 1996). Even the land-sea contrast with higher values over land, traditionally interpreted as the effect of fractionation during continental recycling (Gat and Matsui, 1991), is well captured by the model even without representing this process. The latitudinal structure, with a local minimum near the equator, maxima in the subtropics, a strong poleward decrease in mid-latitudes, and a poleward increase in high latitudes ($> 60^{\circ}$), are well captured (Fig. 3). The root mean square error is only 3.2 ‰ globally.

It is surprising that LMDZ simulates the latitudinal gradient of precipitation d-excess well, while it had difficulties simulating it in the vapor. In particular in the subtropics,

CPD
8, 5493–5543, 2012

precipitation d-excess has the right mean value in spite of the vapor d-excess being underestimated by about 20 ‰ (Sect. 3.1). It could be that d-excess in precipitation reflects the d-excess in the vapor at a level where LMDZ would agree better with observations, if such observations existed. It could also be that the correct values of precipitation d-excess arises from a compensation of errors. For example, the parameter ϕ controlling kinetic fractionation during rain re-evaporation was tuned to optimize, among other targets, precipitation d-excess (Risi et al., 2010b).

No coherent spatial pattern for ^{17}O-excess emerges from the sparse data available. Measured values range from about 0 to 50 permeg. The values simulated by LMDZ are within this range, except in Antarctica and Greenland where values are underestimated by about 40 permeg. Outside these two regions, the root mean square error is 13 permeg. The underestimate of ^{17}O-excess in subtropical water vapor source (Sect. 3.1) could contribute to the underestimate of polar ^{17}O-excess. As will be detailed in Sect. 4.3.3, uncertainties in supersaturation parameter λ and in the equilibrium fractionation and diffusivity coefficients may also contribute to LMDZ difficulties in simulating polar ^{17}O-excess.

3.3 Seasonnal variations

The simulated latitudinal pattern of seasonal variations (JJA-DJF) in δ^{18}O, d-excess and ^{17}O-excess are compared with observations in Fig. 4. The seasonality in δ^{18}O is very well captured by the model, with a root mean square error is 2.7 ‰. In the tropics, precipitation is more depleted during the wet season, consistent with the amount effect. Poleward of 35° latitude, precipitation is more depleted in winter, consistent with the temperature effect (Dansgaard, 1964).

The broad pattern of d-excess seasonality is well captured. In most regions of the globe, observed d-excess is lower in summer of each hemisphere, especially in the subtropics. This is also the case in LMDZ, but with less noise. The root mean square error is 4.8 ‰. The d-excess seasonality in high latitudes has often been interpreted as the effect of evaporative conditions at the moisture source (e.g. Delmotte et al., 2000).

CPD
8, 5493–5543, 2012

The underestimation of the d-excess sensitivity to evaporative conditions (Sect. 3.1) does not prevent LMDZ to capture the observed d-excess seasonality in northern high latitudes. However, LMDZ fails to simulate the higher d-excess in winter in Central Antarctica. As will be detailed in Sect. 4.3.3, this could be associated with uncertainties in the parameter λ.

We have only three sites where seasonal cycles of ^{17}O-excess in precipitation are available: in Greenland, Antarctica and Bolivia. Observed ^{17}O-excess is 15 permeg lower in summer in Greenland, a few permeg higher in winter in Antarctica, and 22 permeg lower during the dry season in Bolivia. LMDZ fails at capturing the correct seasonality at all sites.

Simulated d-excess and ^{17}O-excess in tropical regions are very sensitive to the choice of the parameter ϕ. Figure 5 shows the sensitivity of δ^{18}O, d-excess and ^{17}O-excess to this parameter. When $\phi = 0$, the relative humidity around rain drops is that of the environment and kinetic fractionation is stronger. In this case, δ^{18}O increases and d-excess and ^{17}O-excess decrease especially in dry regions. Over the Bolivian site however, tuning ϕ is not sufficient to reach model-data agreement. In observations, ^{17}O-excess is 22 permeg lower during the dry season than during the wet season, possibly due to more rain re-evaporation during the dry season. But when $\phi = 0$ (respectively 0.9), ^{17}O-excess is only 3 permeg (respectively 0 permeg) during the dry season than during the wet season. Some other processes are probably at play in this region that LMDZ does not capture. For example, the 4 ‰ higher d-excess during the dry season can be associated with a higher proportion of the moisture arising from bare soil evaporation upstream, which is characterized by higher d-excess (Gat and Matsui, 1991). LMDZ does not simulate this effect.

3.4 Last glacial maximum

LGM-PD variations for δ^{18}O and d-excess were extensively evaluated in Risi et al. (2010b). We focus here on LGM-PD variations in Antarctica where most of the LGM ^{17}O-excess data are available. LMDZ simulates qualitatively well the observed

CPD
8, 5493–5543, 2012

depletion at LGM in Antarctica, and it captures the increased depletion towards the interior (Fig. 6a). However, the depletion magnitude is underestimated by 20 % in Dome C and up to 45 % in Vostok and Taylor Dome (Table 3).

Although simulating d-excess signals with the same sign as $\delta^{18}O$ has proven difficult for some models (Werner et al., 2001; Noone, 2008), LMDZ is able to simulate the lower d-excess at LGM over most of Antarctica (Fig. 6b). In observations, the decrease of d-excess from PD to LGM is all the larger as we go poleward. However, LMDZ simulates the opposite, with an increase over Central Antarctica from PD to LGM.

LMDZ captures the lower ^{17}O-excess observed at LGM at most sites (Fig. 6c). In observations, the decrease of ^{17}O-excess from PD to LGM is all the larger as we go poleward, as for d-excess. This is also well captured by LMDZ. However, LMDZ overestimates the ^{17}O-excess decrease from PD to LGM at all sites, and simulates the wrong sign near the coast.

4 Understanding what controls precipitation ^{17}O-excess

We now use LMDZ simulations to understand what controls $\delta^{18}O$, d-excess and ^{17}O-excess in the model. In doing so, we keep in mind the strengths and weaknesses highlighted by the model-data comparison: we have good confidence in the $\delta^{18}O$ distribution both for PD and LGM. We have relatively good confidence in the annual-mean d-excess distribution and in the broad latitudinal pattern of d-excess seasonality. Finally, we have moderate confidence in the LGM-PD changes in d-excess and ^{17}O-excess in Antarctica. All other features are subject to more caution, as they are either mis-represented in LMDZ, or difficult to evaluate given the lack of data.

Figure 7 shows the decomposition of the latitudinal variations of annual mean $\delta^{18}O$, d-excess and ^{17}O-excess into four effects (Sect. 2.4): (1) precipitation-vapor difference (green); (2) evaporative conditions associated with SST and rh_s (orange); (3) effect of supersaturation (dashed pink) and (4) all other processes (red). The sum of all these

CPD
8, 5493–5543, 2012

contributions make the total signal (black). Figures 8 and 9 shows the same decomposition for seasonal and LGM-PD variations respectively.

4.1 Precipitation-vapor difference

The contribution of precipitation-vapor difference to the precipitation signal is shown in green in Figs. 7–9.

4.1.1 Rain re-evaporation

In the tropics, in the absence of rain re-evaporation, the precipitation reequilibrates with the vapor as it falls (Risi et al., 2008a). Variations in precipitation-vapor difference are thus mainly associated with rain re-evaporation: as rain re-evaporates, $\delta^{18}O$ increases and d-excess and ^{17}O-excess decrease in the rain (Risi et al., 2008a, 2010a; Lee and Fung, 2008; Barras and Simmonds, 2009; Landais et al., 2010). For $\delta^{18}O$, this process is the main reason for the so-called amount effect (Risi et al., 2008a), i.e. the decrease of $\delta^{18}O$ as precipitation amount increases. In the tropics, the green and black curves have similar shapes for $\delta^{18}O$ and ^{17}O-excess, and to a lesser extent for d-excess (Fig. 7). This means that rain re-evaporation explains much of the latitudinal variations in precipitation isotopic composition. In particular, rain re-evaporation explains the slight local minimum in $\delta^{18}O$ in the equatorial region (around 0° N) where the air is moist, and the larger values in the subtropics (around 30° N and 35° S) where re-evaporation is strong (Fig. 7a). Consistently, it also explains the local maxima in d-excess and ^{17}O-excess in the equatorial region and the lower values in the subtropics (Fig. 7b, c).

Regarding seasonality, in the tropics, the green and black curves also have a similar shape for $\delta^{18}O$ and ^{17}O-excess, and to a lesser extent for d-excess (Fig. 8). This means that the effect of rain re-evaporation dominates the seasonality in $\delta^{18}O$, with larger values in the dry season (Fig. 8a), and the seasonality in ^{17}O-excess (and to a lesser extent d-excess), with lower values during the dry season (Fig. 8b, c). This seasonal evolution of the triple isotopic composition of precipitation is consistent with

CPD
8, 5493–5543, 2012

that observed during the transition from dry to wet season in the Sahel (Risi et al., 2008b; Landais et al., 2010).

At LGM, LMDZ simulates little change in $\delta^{18}O$, d-excess and ^{17}O-excess, but the latitudinal distribution of the small changes mirror those in precipitation-vapor difference.

4.1.2 Effect of fractionation coefficients

In high latitudes, precipitation falls as snow and is thus not affected by post-condensational processes. The precipitation-vapor difference is thus associated with condensation processes. As temperature decreases, the fractionation coefficients increase, but the coefficient for $\delta^{18}O$ increases faster than that for δD. Therefore, precipitation-vapor difference for d-excess becomes more negative at colder temperatures. This contributes to the lower d-excess in polar regions, during winter and during the LGM (Fig. 7b, 8b and 9b). During winter, this effect is not major and does not prevent d-excess to be higher in winter. During the LGM in contrast, this effect appears as the main process contributing to the lower d-excess in polar regions.

Similarly, the precipitation-vapor difference in ^{17}O-excess increases at lower temperatures. This is due to the fact that the slope of the meteorologic water line (0.528) is lower than the logarithm of the ratio of the fractionation coefficients ($\frac{\ln(\alpha_{O17})}{\ln(\alpha_{O18})} = 0.529$). This contributes to increase ^{17}O-excess in polar regions, in winter and at LGM. This effect might however be overestimated in LMDZ. Observations at the NEEM station in Greenland shows that ^{17}O-excess is only 3 ± 13 permeg higher in the snow than in the vapor (Landais et al., 2012b), compared to 41 permeg higher as predicted by LMDZ (not shown). This may be due to $\frac{\ln(\alpha_{O17})}{\ln(\alpha_{O18})}$ being actually closer to 0.528 than to 0.529 for vapor-solid equilibrium (Landais et al., 2012b). However, even in LMDZ, this equilibrium fractionation effect is not dominant since it is overwhelmed by other effects (green and black curves do not have similar shapes and often have opposite signs on Figs. 7c, 8c and 9c).

CPD
8, 5493–5543, 2012

4.2 Evaporative conditions

The contribution of evaporative conditions (SST and rh_s) to the precipitation signal is shown in orange in Figs. 7–9. The role of rh_s only is shown in dashed orange. The difference between the solid and dashed lines correspond to the role of SST only. For ^{17}O-excess, the solid and dashed orange lines are identical, since SST has no impact on ^{17}O-excess at evaporation (Risi et al., 2010c).

The poleward decrease in d-excess from 30° to 60° in the Southern Ocean is due to evaporative conditions (Fig. 7b). SST and rh_s account each for about half of this decrease. For ^{17}O-excess, LMDZ simulates a small role for evaporative conditions in the latitudinal gradient (Fig. 7c). This is consistent with the small simulated slope of ^{17}O-excess as a function of rh_s (Sect. 3.1). In nature, the role for evaporative conditions might be stronger.

The broad latitudinal distribution of d-excess seasonality was characterized both in observations and LMDZ by lower values in summer in the subtropics and mid-latitudes of each hemisphere (Sect. 3, Fig. 4). This pattern is similar to that of the evaporative condition contribution, in particular the effect of rh_s at the moisture source (Fig. 8b). Therefore, the observed d-excess pattern could be due to the rh_s seasonality at the moisture source or seasonal shifts in moisture sources. In high latitudes, the contributions of distillation (red) and supersaturation (pink) effects are large and largely compensate each other (later discussion in Sect. 4.3). Beside these two components, the dominant cause for d-excess seasonality in polar regions is rh_s conditions at the moisture source (Fig. 8b). The importance of evaporative conditions could be even stronger in nature than in LMDZ, since LMDZ underestimates the effect of rh_s and SST on d-excess.

Evaporative conditions also contribute to the seasonality of δ^{18}O in high latitudes. This is mainly due to the rh_s being drier in summer.

In LMDZ, changes in evaporative conditions play little role in decreasing d-excess at LGM. This is because rh_s and SST do not vary as much between LGM and present

CPD
8, 5493–5543, 2012

as during a seasonal cycle. This contradicts the suggestion that higher rh_s at the LGM (Jouzel et al., 1982) or lower SST at the moisture source (Stenni et al., 2001) contribute to the lower d-excess in Antarctica. It is possible that the contribution of evaporative conditions was significant at LGM, that it is underestimated by LMDZ, and that LMDZ gets the right sign of d-excess change through compensation of errors. This study just shows that the lower d-excess at LGM can be explained without change in evaporative conditions, provided that a significant supersaturation parameter is chosen.

For ^{17}O-excess, the evaporative condition effect at LGM is not negligeable in Antarctica. The effect of rh_s at the moisture source leads to lower ^{17}O-excess by 5 permeg at Vostok. If LMDZ had a more realistic rh_s-^{17}O-excess slope (i.e. about 4 times larger), the rh_s contribution might have been larger, in better agreement with Landais et al. (2008). LMDZ can however simulate the observed lower ^{17}O-excess at LGM without an important role of evaporative conditions, provided that an adequate supersaturation parameter is used (Sect. 4.3.3).

4.3 Supersaturation and other processes

The effect of supersaturation is shown in dashed pink in Figs. 7–9. The sum of all effects other than supersaturation, precip-vapor difference and evaporative conditions is shown in red.

4.3.1 Convective processes

In the tropics, the air temperature is relatively uniform horizontally (Sobel and Bretherton, 2000) so the temperature effect is small (Rozanski et al., 1993). Large variations in humidity can however be associated with vertical motions (Sherwood, 1996). Since δ^{18}O decreases with altitude, subsidence of air in unsaturated downdrafts of convective systems (Risi et al., 2008a) and the subsidence at the large-scale in dry regions (Frankenberg et al., 2009; Galewsky and Hurley, 2010) both deplete the water vapor. Similarly, subsidence is expected to increase d-excess due to its expected increase

CPD
8, 5493–5543, 2012

with altitude (Bony et al., 2008; Sayres et al., 2010). In addition, rain re-evaporation and rain-vapor interactions in moist conditions can also deplete the vapor (Lawrence et al., 2004; Worden et al., 2007) and increase the d-excess and ^{17}O-excess of the vapor (Landais et al., 2010). Therefore, in the tropics, the red curves in Figs. 7–9 correspond to the combined effects of large-scale dynamics, of unsaturated dowdrafts and of rain re-evaporation on the vapor. We can see that these effects are the major contribution to explain the maximum of d-excess in equatorial convective regions (Fig. 7b). They are also a major contribution to the seasonality in δ^{18}O, d-excess and ^{17}O-excess in the tropics (Fig. 8). This is consistent with the important role of unsaturated downdrafts in the amount effect (Risi et al., 2008a).

4.3.2 Distillation and mixing

In high latitudes, the above-mentioned processes play a minor role. Therefore, the red curves represent the combined effects of distillation, evaporative recycling along trajectories and mixing between air masses. Distillation at low temperatures decreases δ^{18}O and increases d-excess. Simple Rayleigh distillation calculations based on LMDZ temperature show that if there was only distillation, the δ^{18}O latitudinal gradient would be 4 times larger than actually simulated (Fig. 7a, blue). This is because the δ^{18}O decrease by Rayleigh distillation is dampened by evaporative recycling along trajecories. As expected, distillation and mixing processes dominate the δ^{18}O latitudinal gradient, consistent with the traditional temperature effect (Dansgaard, 1964). It also dominates the seasonality in δ^{18}O and the LGM-PD difference.

For d-excess, the polar increase of the red contribution (Fig. 7b) is associated with Rayleigh distillation, which increases d-excess at low temperatures (Jouzel and Merlivat, 1984). For the same reasons, in high latitudes, the Rayleigh effect contributes to the increased d-excess in winter (Fig. 8b) and at LGM (Fig. 9b).

For ^{17}O-excess, the poleward decrease of the red contribution in high latitudes (Fig. 7c) may be due to the effect of evaporative recycling. The effect of evaporative recycling on ^{17}O-excess is due to the fact that mixing of two air masses with very

CPD
8, 5493–5543, 2012

different $\delta^{18}O$ leads to ^{17}O-excess values that are lower than both end-members (Risi et al., 2010c). This explains why the red curve contributes to lower ^{17}O-excess in high latitudes (Fig. 7).

4.3.3 Supersaturation

In polar regions, the distillation effect is partially compensated by the supersaturation effect. With supersaturation at low temperature, $\delta^{18}O$ decreases less and d-excess and ^{17}O-excess increase less along trajectories. The supersaturation effect has little effect on $\delta^{18}O$ (Fig. 7a, pink). For d-excess and ^{17}O-excess, the distillation/mixing and supersaturation effects are both very large and largely compensate each other. The sign of the seasonality and of LGM-PD variations thus results from a subtle balance between distillation effects and supersaturation effects. In Greenland where LMDZ captures the sign of the d-excess seasonality, the distillation effect dominates and this leads to higher d-excess values in winter when the distillation is stronger. In Vostok in contrast, d-excess is higher in winter in observations but lower in winter in LMDZ. This suggests that in observations, the distillation effect dominates, but that in LMDZ, the supersaturation effect is too strong and dominates. In observations, ^{17}O-excess is higher in winter in Greenland and lower in winter in Antarctica. This suggests that the supersaturation effect dominates in Antarctica but not in Greenland. In LMDZ, the seasonality is misrepresented in both regions.

As a consequence of the subtle balance between distillation effects and supersaturation effects, d-excess and ^{17}O-excess in polar regions is extremely sensitive to the choice of λ, consistent with simple model studies (Ciais and Jouzel, 1994; Winkler et al., 2012b; Landais et al., 2012a,b). λ was chosen to optimize the latitudinal gradient in polar d-excess (Risi et al., 2010b). If λ was lower, the agreement would be better for ^{17}O-excess, but d-excess would be over-estimated in Central Antarctica (Fig. 10b,c). In LMDZ, we cannot tune λ to agree both with d-excess and ^{17}O-excess. The sensitivity to a poorly-constrained parameter makes the interpretation of d-excess and ^{17}O-excess

CPD
8, 5493–5543, 2012

LGM-PD changes difficult. Any observed change at a given location can be reproduced by any model by tuning λ. Setting $\lambda = 0.004$ leads to a good agreement with the LGM-PD variations, but a lower value of λ can lead to a reversal of the sign of the d-excess and ^{17}O excess LGM-PD variations (Fig. 10e,f).

In addition to the uncertainty on λ, there are also uncertainties on the equilibrium coefficients and on diffusivities. First, there is persistent uncertainty on vapor-solid fractionation at very low temperature. Vapor-solid fractionation coefficients have been measured only down to −34 °C and are extrapolated beyond (Majoube, 1971a), leading to some uncertainty. There are also disagreements between different experimental measurements (Ellehoej, 2011). Second, there is uncertainties on the diffusivity coefficients. Cappa et al. (2003) and Merlivat and Jouzel (1979) found different values and Luz et al. (2009) suggest that they may actually vary also with temperature. Therefore, the combined uncertainties on supersaturation, equilibrium fractionation and diffusivity coefficients, make it difficult to interpret d-excess and ^{17}O-excess data and to identify the culprit in the shortcomings of the d-excess and ^{17}O-excess simulation in polar regions.

5 Conclusion and perspectives

We used the LMDZ GCM to simulate the PD and LGM distributions of precipitation δ^{18}O, d-excess and ^{17}O-excess. LMDZ captures very well the δ^{18}O distribution and climatic variations. After appropriate tuning of supersaturation, it captures reasonably well the d-excess distribution and the average LGM-PD variations in Antarctica. For ^{17}O-excess, the lack of data makes it difficult to evaluate the spatio-temporal distribution. LMDZ underestimates the ^{17}O-excess latitudinal gradient in the Austral Ocean water vapor and exhibits caveats in its simulation of seasonal variations on some stations.

We propose a methodology to quantify the controling factors of the associated latitudinal, seasonal and LGM-PD variations. Table 5 summarizes the main factor controlling

CPD
8, 5493–5543, 2012

the different aspects of the $\delta^{18}O$, d-excess and ^{17}O-excess spatio-temporal distribution depending on latitude. In the tropics, rain re-evaporation and convective processes explain the main features of the $\delta^{18}O$, d-excess and ^{17}O-excess spatio-temporal distributions. In mid and high-latitude, as expected distillation effect is the first order control on $\delta^{18}O$. D-excess and ^{17}O-excess are also affected by distillation, but also by other processes. Evaporative conditions play a role for d-excess, and may also play a role for ^{17}O-excess if LMDZ was more sensitive to rh_s and SST. The sensitivity to evaporative conditions is an added value of d-excess compared to $\delta^{18}O$, consistent with previous studies (e.g. Vimeux et al., 1999, 2001b; Gat, 2000; Stenni et al., 2001; Masson-Delmotte et al., 2005). ^{17}O-excess also features this added value, but an additional particularity is its sensitivity to mixing along distillation trajectories. ^{17}O-excess seems to be sensitive to a much broader range of processes. Determining the controling factors in nature with more confidence would however require much more data to more comprehensively evaluate GCM simulations of ^{17}O-excess.

Supersaturation effects play a major role on both d-excess and ^{17}O-excess, leading to a large uncertainty in their interpretation. At LGM in polar region for both d-excess and ^{17}O-excess, distillation, transport and mixing effects push towards higher values while supersaturation effects push towards lower values. The balance between these two large effects is subtle and very sensitive to the assumed supersaturation function. Using a supersaturation function that leads to d-excess and ^{17}O-excess consistent with PD observations, LMDZ is able to simulate the lower d-excess and ^{17}O-excess at LGM without requiring any effect of changes in evaporative conditions at the moisture source. The choice of the supersaturation function, together with uncertainties in equilibrium fractionation and diffusivity coefficients, remain a key uncertainty in interpreting d-excess and ^{17}O-excess, since its choice determines the sign of LGM-PD changes. Measurements of vapor and precipitation along Antarctica transects would be very helpful to better constrain this function.

We acknowledge the limitations inherent to our GCM simulations. The sensitivity of d-excess and ^{17}O-excess to ocean evaporative conditions is underestimated, for reasons

CPD
8, 5493–5543, 2012

that we do not understand but that are more likely related to free tropospheric processes. Vertical profiles of ^{17}O-excess or latitudinal gradients in the free troposphere would be helpful to diagnose the cause of these problems. Alternatively, multi-model comparison with other isotopic GCMs that do not feature the same bias, if these exist, could provide some insight. Finally, taking into account fractionating evaporation over land may be necessary to interpret d-excess and ^{17}O-excess patterns over land. The methodology presented here to decompose the isotopic signals into the different physical processes will remain valid for all GCMs. It will be worth applying it to other GCMs to extract robust features, and applying it to future versions of GCMs in which the simulation of d-excess and ^{17}O-excess will improve.

Appendix A

Predicting the isotopic composition of the boundary layer vapor using the closure assumption

The simplest equation to predict the isotopic composition of the boundary layer vapor is the Merlivat and Jouzel (1979) closure. Although it fails to predict the absolute values of δ^{18}O and d-excess (Jouzel and Koster, 1996), it has been shown to accurately predict the sensitivity of the isotopic composition to ocean surface conditions (Uemura et al., 2008, 2010; Risi et al., 2010c). We recall here the derivation of this equation and the underlying assumptions.

The isotopic composition R_E of the evaporation flux from the ocean is given by the Craig and Gordon (1965) equation:

$$R_E = \frac{1}{\alpha_K} \cdot \frac{R_{oce}/\alpha_{eq} - rh_s \cdot R_v}{1 - rh_s} \quad \text{(A1)}$$

where α_K is the kinetic fractionation coefficient, α_{eq} is the liquid-vapor equilibrium fractionation coefficient and R_{oce} is the isotopic ratio of the ocean surface. The relative

CPD
8, 5493–5543, 2012

humidity at the surface, rh_s is the relative humidity of near surface air at the temperature of the ocean surface T_s:

$$rh_s = rh_a \cdot \frac{q_{sat}(T_a)}{q_{sat}(T_s)} \quad \text{(A2)}$$

where q_{sat} is the specific humidity at saturation and rh_a and T_a are the relative humidity and temperature of the near-surface air respectively.

If we assume that (1) the only source of vapor in the boundary layer is the surface evaporation and (2) the sinks of vapor from the boundary layer do not fractionate (i.e. have the composition of the boundary layer, e.g. air flux going out of the boundary layer), then at stationary state $R_v = R_E$. Combined with Eq. (A1), this leads to (Merlivat and Jouzel, 1979):

$$R_v = \frac{R_{oce}}{\alpha_{eq} \cdot (\alpha_K + rh_s \cdot (1 - \alpha_K))} \quad \text{(A3)}$$

Applying this equation to $H_2^{18}O$, $H_2^{18}O$ and HDO isotopic ratios, it can be shown that d-excess in the boundary layer vapor increases with SST and that d-excess and ^{17}O-excess decrease with rh_s.

Acknowledgements. We thank Boaz Luz, Eugeni Barkan and Ryu Uemura for sharing their ^{17}O-excess data.

The publication of this article is financed by CNRS-INSU.

References

Barkan, E. and Luz, B.: High precision measurements of $^{17}O/^{16}O$ and $^{18}O/^{16}O$ ratios in H_2O, Rapid Commun. Mass Sp., 19, 3737–3742, 2005. 5498

Barkan, E. and Luz, B.: Diffusivity fractionations of $H_2^{16}O/H_2^{17}O$ and $H_2^{16}O/H_2^{18}O$ in air and their implications for isotope hydrology, Rapid Commun. Mass Sp., 21, 2999–3005, 2007. 5495, 5498

Barras, V. and Simmonds, I.: Observation and modelling of stable water isotopes as diagnostics of rainfall dynamics over Southeastern Australia, J. Geophys. Res., 114, D23308, doi:10.1029/2009JD012132, 2009. 5510

Bartlein, P. J., Harrison, S. P., Brewer, S., Connor, S., Davis, B. A. S., Gajewski, K., Guiot, J., Harrison-Prentice, T. I., Henderson, A., Peyron, O., Prentice, I. C., Scholze, M., Seppä, H., Shuman, B., Sugita, S., Thompson, R. S., Viau, A. E., Williams, J., and Wu, H.: Pollen-based continental climate reconstructions at 6 and 21 ka: a global synthesis, Clim. Dynam., 37, 775–802, doi:10.1007/s00382-010-0904-1, 2010. 5499

Bony, S. and Emanuel, K. A.: A parameterization of the cloudiness associated with cumulus convection, evaluation using TOGA COARE data, J. Atmos. Sci., 58, 3158–3183, 2001. 5497

Bony, S., Risi, C., and Vimeux, F.: Influence of convective processes on the isotopic composition (δO^{18} and δD) of precipitation and water vapor in the Tropics, Part 1: radiative-convective equilibrium and TOGA-COARE simulations, J. Geophys. Res., 113, D19305, doi:10.1029/2008JD009942, 2008. 5498, 5499, 5514

Braconnot, P., Otto-Bliesner, B., Harrison, S., Joussaume, S., Peterchmitt, J.-Y., Abe-Ouchi, A., Crucifix, M., Driesschaert, E., Fichefet, Th., Hewitt, C. D., Kageyama, M., Kitoh, A., Laîné, A., Loutre, M.-F., Marti, O., Merkel, U., Ramstein, G., Valdes, P., Weber, S. L., Yu, Y., and Zhao, Y.: Results of PMIP2 coupled simulations of the Mid-Holocene and Last Glacial Maximum – Part 1: experiments and large-scale features, Clim. Past, 3, 261–277, doi:10.5194/cp-3-261-2007, 2007. 5499, 5500

Cappa, C., Hendricks, M., DePaolo, D., and Cohen, R.: Isotopic fractionation of water during re-evaporation, J. Geophys. Res., 108, 4525–4542, 2003. 5516

Ciais, P. and Jouzel, J.: Deuterium and oxygen 18 in precipitation: isotopic model, including cloud processes, J. Geophys. Res., 99, 16793–16803, 1994. 5515

CLIMAP project members: Seasonal reconstructions of the Earth's surface at the last glacial maximum, Geol. Soc. Am., Map Chart Ser. MC-36, 1981. 5500

CPD
8, 5493–5543, 2012

Craig, H. and Gordon, L. I.: Deuterium and oxygen-18 variations in the ocean and marine atmosphere, Stable Isotope in Oceanographic Studies and Paleotemperatures, edited by: Tongiorgi, E., 9–130, Pisa: Lab. Geol. Nucl., 1965. 5497, 5504, 5518

Dansgaard, W.: Stable isotopes in precipitation, Tellus, 16, 436–468, 1964. 5495, 5506, 5507, 5514

Delaygue, G.: Relations entre surface océanique et composition isotopique des précipitations antarctiques: simulations pour différents climats, Ph. D. thesis, Université d'Aix-Marseille III, France, 2000. 5496

Delmotte, M., Masson, V., Jouzel, J., and Morgan, V.: A seasonal deuterium excess signal at Law Dome, coastal Eastern Antarctica: a southern ocean signature, J. Geophys. Res., 105, 7187–7197, 2000. 5507

Ellehoej, M.: Ice-vapor equilibrium fractionation factor experimental investigations and possible impacts on the understanding of the hydrological cycles on Earth and Mars, Ph. D. thesis, University of Copenhagen, Denmark, 2011. 5516

Emanuel, K. A.: A scheme for representing cumulus convection in large-scale models, J. Atmos. Sci., 48, 2313–2329, 1991. 5497

Emanuel, K. A. and Zivkovic-Rothman, M.: Development and evaluation of a convection scheme for use in climate models, J. Atmos. Sci., 56, 1766–1782, 1991. 5497

Farrera, I., Harrison, S. P., Prentice, I. C., Ramstein, G., Guiot, J., Bartlein, P. J., Bonnefille, R., Bush, M., Cramer, W., von Grafenstein, U., Holmgren, K., Hoohiemstra, H., Hope, G., Jolly, D., Lauritzen, S.-E., Ono, Y., Pinot, S., Stute, M., and Yu, G.: Tropical climates at the Last Glacial Maximum: a new synthesis of terrestrial palaeoclimate data, part I: vegetation, lake-levels and geochemistry, Clim. Dynam., 15, 823–856, 1999. 5499

Fekete, B., Gibson, J., Aggarwal, P., and Vorosmarty, C. J.: Application of isotope tracers in continental scale hydrological modeling, J. Hydrol., 330, 444–456, 2006. 5529

Frankenberg, C., Yoshimura, K., Warneke, T., Aben, I., Butz, A., Deutscher, N., Griffith, D., Hase, F., Notholt, J., Schneider, M., Schrijver, H., and Röckmann, T.: Dynamic processes governing lower-tropospheric HDO/H_2O ratios as observed from space and ground, Science, 325, 1374–1377, 2009. 5513

Galewsky, J. and Hurley, J. V.: An advection-condensation model for subtropical water vapor isotopic ratios, J. Geophys. Res., 115, D16115, doi:10.1029/2009JD013651, 2010. 5513

Gat, J. R.: Atmospheric water balance-the isotopic perspective, Hydrol. Process., 14, 1357–1369, 2000. 5517

CPD
8, 5493–5543, 2012

Gat, J. R. and Matsui, E.: Atmospheric water balance in the Amazon Basin: an isotopic evapotranspiration model, J. Geophys. Res., 96, 13179–13188, 1991. 5506, 5508
Gat, J. R., Shemesh, A., Tziperman, E., Hecht, A., Georgopoulos, D., and Basturk, O.: The stable water isotope composition of waters in the Eastern Mediterranean Sea, J. Geophys. Res., 101, 6441–6451, 1996. 5506
Gates, W. L.: AMIP: the atmospheric model intercomparison project, B. Am. Meteor. Soc., 73, 1962–1970, 1992. 5499
Hendricks, M., DePaolo, D., and Cohen, R.: Space and time variation of δ^{18}O and δD: can paelotemperatures be estimated from ice cores?, Glob. Geochem. Cy., 14, 851–861, 2000. 5495
Hoffmann, G., Werner, M., and Heimann, M.: Water isotope module of the ECHAM atmospheric general circulation model: a study on timescales from days to several years, J. Geophys. Res., 103, 16871–16896, 1991. 5500
Hourdin, F. and Armengaud, A.: The use of finite-volume methods for atmospheric advection of trace species, Part I: test of various formulations in a general circulation model, Mon. Weather Rev., 127, 822–837, 1999. 5497
Hourdin, F., Musat, I., Bony, S., Braconnot, P., Codron, F., Dufresne, J.-L., Fairhead, L., Filiberti, M.-A., Friedlingstein, P., Grandpeix, J.-Y., Krinner, G., Levan, P., Li, Z.-X., and Lott, F.: The LMDZ4 general circulation model: climate performance and sensitivity to parametrized physics with emphasis on tropical convection, Clim. Dynam., 27, 787–813, 2006. 5497
Johnsen, S., Dansgaard, W., Clausen, H., and Langway, J. C.: Oxygen isotope profiles through the Antarctic and Greenland ice sheets, Nature, 235, 429–434, 1972. 5495
Johnson, D. G., Jucks, K. W., Traub, W. A., and Chance, K. V.: Isotopic composition of stratospheric water vapor: implications for transport, J. Geophys. Res., 106, 12219–12226, 2001. 5498
Joussaume, S. and Taylor, K. E.: Status of the paleoclimate modeling intercomparison project, in: Proceedings of the first international AMIP scientific conference, WCRP-92, Monterey, 15–19 May 1995, USA, 425–430, 1995. 5500
Jouzel, J.: Water stable isotopes: atmospheric composition and applications in polar ice core studies, Treatise on Geochemistry, 4, 213–243, 2003. 5495
Jouzel, J. and Koster, R. D.: A reconsideration of the initial conditions used for stable water isotope models, J. Geophys. Res., 101, 22933–22938, 1996. 5518

CPD
8, 5493–5543, 2012




Jouzel, J. and Merlivat, L.: Deuterium and oxygen 18 in precipitation: modeling of the isotopic effects during snow formation, J. Geophys. Res., 89, 11749–11757, doi:10.1029/JD089iD07p11749, 1984. 5495, 5497, 5514

Jouzel, J., Merlivat, L., and Lorius, C.: Deuterium excess in an East Antarctic ice core suggests higher relative humidity at the oceanic surface during the last glacial maximum, Nature, 299, 688–691, 1982. 5495, 5513

Kendall, C. and Coplen, T. B.: Distribution of oxygen-18 and deuterium in river waters across the United States, Hydrol. Process., 15, 1363–1393, 2001. 5500, 5529

Landais, A., Barkan, E., and Luz, B: The triple isotopic composition of oxygen in leaf water, Geochim. Cosmochim. Ac., 70, 4105–4115, 2006. 5501

Landais, A., Barkan, E., and Luz, B.: Record of $\delta^{18}O$ and ^{17}O-excess in ice from Vostock Antarctica during the last 150 000 years, Geophys. Res. Lett., 35, L02709, doi:10.1029/2007GL032096, 2008. 5495, 5496, 5501, 5503, 5504, 5513, 5530, 5531

Landais, A., Risi, C., Bony, S., Vimeux, F., Descroix, L., Falourd, S., and Bouygues, A.: Combined measurements of ^{17}O-excess and d-excess in African monsoon precipitation: implications for evaluating convective parameterizations, Earth Planet. Sci. Lett., 298, 104–112, 2010. 5496, 5498, 5501, 5510, 5511, 5514, 5530

Landais, A., Ekaykin, A., Barkan, E., Winkler, R., and Luz, B.: Seasonal variations of ^{17}O-excess and d-excess in snow precipitation at Vostok station, East Antarctica, J. Glaciol., 58, 725–733, doi:10.3189/2012JoG11J237, 2012a. 5495, 5498, 5501, 5515

Landais, A., Steen-Larsen, H.-C., Guillevic, M., Masson-Delmotte, V., Vinther, B., and Winkler, R.: Triple isotopic composition of oxygen in surface snow and water vapor at NEEM (Greenland), Geochim. Cosmochim. Ac., 77, 304–316, 2012b. 5495, 5496, 5498, 5501, 5511, 5515, 5530

Lawrence, J. R., Gedzelman, S. D., Dexheimer, D., Cho, H.-K., Carrie, G. D., Gasparini, R., Anderson, C. R., Bowman, K. P., and Biggerstaff, M. I.: Stable isotopic composition of water vapor in the tropics, J. Geophys. Res., 109, D06115, doi:10.1029/2003JD004046, 2004. 5514

Lee, J.-E. and Fung, I.: "Amount effect" of water isotopes and quantitative analysis of post-condensation processes, Hydrol. Process., 22, 1–8, 2008. 5499, 5510

Lee, J.-E., Fung, I., DePaolo, D. J., and Otto-Bliesner, B.: Water isotopes during the Last Glacial Maximum: new general circulation model calculations, J. Geophys. Res., 113, D19109, doi:10.1029/2008JD009859, 2008. 5496

Lorius, C., Merlivat, L., Jouzel, J., and Pourchet, M.: A 30000 yr isotope climatic record from Antarctic ice, Nature, 280, 644–648, 1979. 5495

Luz, B. and Barkan, E.: Variations of $^{17}O/^{16}O$ and $^{18}O/^{16}O$ in meteoric waters, Geochim. Cosmochim. Ac., 74, 6276–6286, 2010. 5500, 5529, 5530

Luz, B., Barkan, E., Yam, R., and Shemesh, A.: Fractionation of oxygen and hydrogen isotopes in evaporating water, Geochim. Cosmochim. Ac., 73, 6697–6703, 2009. 5516

Majoube, M.: Fractionnement en ^{18}O entre la glace et la vapeur d'eau, J. Chim. Phys., 68, 625–636, 1971a. 5497, 5516

Majoube, M.: Fractionnement en Oxygène 18 et en Deutérium entre l'eau et sa vapeur, J. Chim. Phys., 10, 1423–1436, 1971b. 5497

MARGO project members: Constraints on the magnitude and patterns of ocean cooling at the Last Glacial Maximum, Nat. Geosci., 2, 127–132, 2008. 5500

Marti, O., Braconnot, P., Bellier, J., Benshila, R., Bony, S., Brockmann, P., Cdule, P., Caubel, A., Denvil, S., Dufresne, J.-L., Fairhead, L., Filiberti, M.-A., Foujols, M.-A., Fichefer, T., Friedlingstein, P., Grandpeix, J.-Y., Hourdin, F., Krinner, G., Lévy, C., Madec, G., Musat, I., de Noblet, N., Polcher, J., and Tanlandier, C.: The new IPSL climate system model: IPSL-CM4, Technical report, IPSL, France, 2005. 5497

Masson-Delmotte, V., Jouzel, J., Landais, A., Stievenard, M., Johnsen, S. J., White, J. W. C., Werner, M., Sveinbjornsdottir, A., and Fuhrer, K.: GRIP Deuterium excess reveals rapid and orbital-scale changes in Greenland moisture origin, Science, 309, 118–121, 2005. 5495, 5517

Masson-Delmotte, V., Hou, S., Ekaykin, A., Jouzel, J., Aristarain, A., Bernardo, R. T., Bromwhich, D., Cattani, O., Delmotte, M., Falourd, S., Frezzotti, M., Gallée, H., Genoni, L., Isaksson, E., Landais, A., Helsen, M., Hoffmann, G., Lopez, J., Morgan, V., Motoyama, H., Noone, D., Oerter, H., Petit, J., Royer, A., Uemura, R., Schmidt, G., Schlosser, E., Simes, J., Steig, E., Stenni, B., Stievenard, M., van den Broeke, M., van de Wal, R., van den Berg, W.-J., Vimeux, F., and White, J.: A review of Antarctic surface snow isotopic composition: observations, atmospheric circulation and isotopic modelling, J. Climate, 21, 3359–3387, 2008. 5495, 5500

Masson-Delmotte, V., Braconnot, P., Hoffmann, G., Jouzel, J., Kageyama, M., Landais, A., Lejeune, Q., Risi, C., Sime, L., Sjolte, J., Swingedouw, D., and Vinther, B.: Sensitivity of interglacial Greenland temperature and $\delta^{18}O$: ice core data, orbital and increased CO_2 climate simulations, Clim. Past, 7, 1041–1059, doi:10.5194/cp-7-1041-2011, 2011. 5496

CPD
8, 5493–5543, 2012

Meehl, G. A., Covey, K., Delworth, T., Latif, M., McAvaney, B., Mitchell, J. F. B., Stouffer, R. J., and Taylor, K.: The WCRP CMIP3 multimodel dataset: a new era in climate change research, B. Am. Meteor. Soc., 7, 1383–1394, 2007. 5497

Merlivat, L. and Jouzel, J.: Global climatic interpretation of the Deuterium-Oxygen 18 relationship for precipitation, J. Geophys. Res., 84, 5029–5332, 1979. 5497, 5503, 5504, 5516, 5518, 5519, 5532, 5534

Merlivat, L. and Nief, G.: Fractionnement isotopique lors des changements d'états solide-vapeur et liquide-vapeur de l'eau à des températures inférieures à 0C, Tellus, 19, 122–127, 1967. 5497

Noone, D.: The influence of midlatitude and tropical overturning circulation on the isotopic composition of atmospheric water vapor and Antarctic precipitation, J. Geophys. Res., 113, D04102, doi:10.1029/2007JD008892, 2008. 5496, 5509

Peltier, W. R.: Ice age paleotopography, Science, 265, 195–201, 1994. 5500

Risi, C., Bony, S., and Vimeux, F.: Influence of convective processes on the isotopic composition (^{18}O and D) of precipitation and water vapor in the Tropics, Part 2: Physical interpretation of the amount effect, J. Geophys. Res., 113, D19306, doi:10.1029/2008JD009943, 2008a. 5503, 5510, 5513, 5514

Risi, C., Bony, S., Vimeux, F., Descroix, L., Ibrahim, B., Lebreton, E., Mamadou, I., and Sultan, B.: What controls the isotopic composition of the African monsoon precipitation? Insights from event-based precipitation collected during the 2006 AMMA campaign, Geophys. Res. Lett., 35, L24808, doi:10.1029/2008GL035920, 2008b. 5506, 5511, 5530

Risi, C., Bony, S., Vimeux, F., Chong, M., and Descroix, L.: Evolution of the water stable isotopic composition of the rain sampled along Sahelian squall lines, Quart. J. Roy. Meteor. Soc., 136, 227–242, 2010a. 5510

Risi, C., Bony, S., Vimeux, F., and Jouzel, J.: Water stable isotopes in the LMDZ4 general circulation model: model evaluation for present day and past climates and applications to climatic interpretation of tropical isotopic records, J. Geophys. Res., 115, D12118, doi:10.1029/2009JD013255, 2010b. 5496, 5497, 5498, 5499, 5500, 5506, 5507, 5508, 5515

Risi, C., Landais, A., Bony, S., Masson-Delmotte, V., Jouzel, J., and Vimeux, F.: Understanding the ^{17}O-excess glacial-interglacial variations in Vostok precipitation, J. Geophys. Res, 115, D10112, doi:10.1029/2008JD011535, 2010c. 5495, 5496, 5503, 5512, 5515, 5518

Risi, C., Bony, S., Ogée, J., Bariac, T., Raz-Yaseed, N., and Wingate, L. Water stable isotopes to evaluate the hydrological budget in large-scale land surface models: investigation with ORCHIDEE-iso, Clim. Dynam., under review, 2012. 5529

Rozanski, K., Araguas-Araguas, L., and Gonfiantini, R.: Isotopic patterns in modern global precipitation, Geophysical Monographs Series, AGU, Climate Change in Continental Isotopic records, edited by: Swart, P. K., et al., AGU, Washington, DC, 78, 1–36, doi:10.1029/GM078p0001, 1993. 5500, 5506, 5513

Sayres, D. S., Pfister, L., Hanisco, T. F., Moyer, E. J., Smith, J. B., Clair, J. M. S., O'Brien, A. S., Witinski, M. F., Legg, M., and Anderson, J. G.: Influence of convection on the water isotopic composition of the tropical tropopause layer and tropical stratosphere, J. Geophys. Res., 11, D00J20, doi:10.1029/2009JD013100, 2010. 5514

Sherwood, S. C.: Maintenance of the free tropospheric tropical water vapor distribution, part II: simulation of large-scale advection, J. Climate, 11, 2919–2934, 1996. 5513

Sobel, A. H. and Bretherton, C. S.: Modeling tropical precipitation in a single column, J. Climate, 13, 4378–4392, 2000. 5513

Steen-Larsen, H.-C., Johnsen, S., Masson-Delmotte, V., Stenni, B., Risi, C., Sodemann, H., Balslev-Clausen, D., Blunier, T., Dahl-Jensen, D., Ellehoej, M., Falourd, S., Gkinis, V., Grindsted, A., Jouzel, J., Popp, T., Sheldon, S., Simonsen, S., Sjolte, J., Steffensen, J., Sperlich, P., Sveinbjornsdottir, A., Vinther, B., and White, J.: Continuous monitoring of summer surface water vapour isotopic composition above the greenland ice sheet, J. Geophys. Res., submitted, 2012. 5504

Stenni, B., Masson-Delmotte, V., Johnsen, S., Jouzel, J., Longinelli, A., Monnin, E., Röthlisberger, R., and Selmo, E.: An oceanic cold reversal during the last deglaciation, Science, 293, 2074–2077, 2001. 5495, 5513, 5517

Stenni, B., Jouzel, J., Masson-Delmotte, V., Röthlisberger, R., Castellano, E., Cattani, O., Falourd, S., Johnsen, S., Longinelli, A., Sachs, J., Selmo, E., Souchez, R., Steffensen, J., and Udisti, R.: A late-glacial high-resolution site and source temperature record derived from the epica dome c isotope records (East Antarctica), Earth Planet. Sci. Lett., 217, 183–195, 2004. 5531

Stewart, M. K.: Stable isotope fractionation due to evaporation and isotopic exchange of falling waterdrops: applications to atmospheric processes and evaporation of lakes, J. Geophys. Res., 80, 1133–1146, 1975. 5498, 5499

Uemura, R., Matsui, Y., Yoshimura, K., Motoyama, H., and Yoshida, N.: Evidence of deuterium-excess in water vapour as an indicator of ocean surface conditions, J. Geophys. Res., 113, D19114, doi:10.1029/2008JD010209, 2008. 5501, 5503, 5518, 5534

Uemura, R., Barkan, E., Abe, O., and Luz, B.: Triple isotope composition of oxygen in atmospheric water vapor, Geophy. Res. Lett., 37, L04402, doi:10.1029/2009GL041960, 2010. 5499, 5501, 5503, 5518, 5534

Uppala, S., Kallberg, P., Simmons, A., Andrae, U., da Costa Bechtold, V., Fiorino, M., Gibson, J., Haseler, J., Hernandez, A., Kelly, G., Li, X., Onogi, K., Saarinen, S., Sokka, N., Allan, R., Andersson, E., Arpe, K., Balmaseda, M., Beljaars, A., van de Berg, L., Bidlot, J., Bormann, N., Caires, S., Chevallier, F., Dethof, A., Dragosavac, M., Fisher, M., Fuentes, M., Hagemann, S., Holm, E., Hoskins, B., Isaksen, L., Janssen, P., Jenne, R., McNally, A., Mahfouf, J.-F., Morcrette, J.-J., Rayner, N., Saunders, R., Simon, P., Sterl, A., Trenberth, K., Untch, A., Vasiljevic, D., Viterbo, P., and Woollen, J.: The ERA-40 re-analysis, Q. J. Roy. Meteor. Soc., 131, 2961–3012, 2005. 5499

Van Hook, A.: Vapor pressures of the isotopic waters and ices, J. Phys. Chem., 72, 1234–1244, doi:10.1021/j100850a028, 1968. 5498

Van Leer, B.: Towards the ultimate conservative difference scheme, IV: a new approach to numerical convection, J. Comput. Phys., 23, 276–299, 1977. 5497

Vimeux, F., Masson, V., Jouzel, J., Stievenard, M., and Petit, J. R.: Glacial-interglacial changes in ocean surface conditions in the Southern Hemisphere, Nature, 398, 410–413, 1999. 5517

Vimeux, F., Masson, V., Delaygue, G., Jouzel, J., Petit, J. R., and Stievenard, M.: A 420 000 year deuterium excess record from East Antarctica: information on past changes in the origin of precipitation at Vostok, J. Geophys. Res., 106, 31863–31873, 2001a. 5503, 5531

Vimeux, F., Masson, V., Jouzel, J., Petit, J.-R., Steig, E., Stievenard, M., Vaikmae, R., and White, J. W.: Holocene hydrological cycle changes in the Southern Hemisphere documented in East antarctic deuterium excess records, Clim. Dynam., 17, 503–513, 2001b. 5517

Vimeux, F., Cuffey, K., and Jouzel, J.: New insights into Southern Hemisphere temperature changes from Vostok ice cores using deuterium excess correction, Earth Planet. Sci. Lett., 203, 829–843, 2002. 5495

Vimeux, F., Gallaire, R., Bony, S., Hoffmann, G., and Chiang, J. C. H.: What are the climate controls on deltaD in precipitation in the Zongo Valley (Bolivia)? Implications for the Illimani ice core interpretation, Earth Planet. Sci. Lett., 240, 205–220, 2005. 5501, 5530

Werner, M., Heimann, M., and Hoffmann, G.: Isotopic composition and origin of polar precipitation in present and glacial climate simulations, Tellus B, 53, 53–71, 2001. 5496, 5509

Winkler, R., Landais, A., Baroni, M., Ekaykin, A., Petit, J. R., Risi, C., Falourd, S., Minster, B., Prie, F., and Jouzel, J.: Inter annual records of δ^{18}O, d-excess and ^{17}O-excess in snow from vostok, East Antarctica, P. Natl. Acad. Sci., under review, 2012a. 5496

Winkler, R., Landais, A., Sodemann, H., Dümbgen, L., Prié, F., Masson-Delmotte, V., Stenni, B., and Jouzel, J.: Deglaciation records of ^{17}O-excess in East Antarctica: reliable reconstruction of oceanic normalized relative humidity from coastal sites, Clim. Past, 8, 1–16, doi:10.5194/cp-8-1-2012, 2012b. 5495, 5496, 5501, 5515, 5530, 5531

Worden, J., Noone, D., and Bowman, K.: Importance of rain evaporation and continental convection in the tropical water cycle, Nature, 445, 528–532, 2007. 5514

Zahn, A., Franz, P., Bechtel, C., Grooß, J.-U., and Röckmann, T.: Modelling the budget of middle atmospheric water vapour isotopes, Atmos. Chem. Phys., 6, 2073–2090, doi:10.5194/acp-6-2073-2006, 2006. 5498

Table 1. Precipitation ^{17}O-excess simulated by LMDZ, compared to data from (Luz and Barkan, 2010) collected in precipitation or rivers. We did not select lakes, caves or pond to avoid samples affected by re-evaporation after rain fall. Based on land surface isotopic modeling (e.g. Fekete et al., 2006; Risi et al., 2012) and observations (Kendall and Coplen, 2001), we assume that river water is close to annual-mean precipitation. For rivers, we thus compare with annual mean simulated precipitation composition. When several samples are taken at the same location in the same season, we present averages.

location	sample type	month	latitude	longitude	^{17}O-excess obs	^{17}O-excess LMDZ
Vienna, Austria	river	Apr	48.23	16.33	18	16.9
Yang Shou, China	river	Oct	24.77	110.5	52	16.5
Montenegro	snow	Jun	42.9	19.3	−12	31.0
Altenahr, Germany	river	Aug	50.52	6.99	27	24.9
Köln, Germany	river	Aug	50.96	6.94	16	22.4
Bacharach, Germany	river	Aug	50.06	7.78	23	24.9
Heidelberg, Germany	river	Aug	49.4	8.73	21	24.9
New Dehli, India	rain	annual	28.58	77.20	22	12.8
Ahamedabad, India	rain	annual	23.00	72.67	20	6.3
Kozhikod, India	rain	annual	11.25	75.72	20	23.5
Borneo, Indonesia	rain	Mar	1.00	114.00	49	25.2
Borneo, Indonesia	rain	Jun–Aug	1.00	114.00	53.5	22.3
Borneo, Indonesia	rain	Nov	1.00	114.00	59	25.9
Jerusalem, Israel	rain	annual	31.78	35.20	35	no rain
Jerusalem, Israel	rain	annual	31.78	35.20	35	no rain
Jerusalem, Israel	spring	Feb	31.78	35.20	51	no rain
Israel	river	Jul	33.23	35.61	55	34.0
Israel	river	Jul	33.23	35.63	53	28.6
Israel	river	Jul	32.88	35.61	36	no rain
New-Zealand	river	Feb	−41	172	47	21.7
New-Zealand	river	Feb	−41	172	56	21.7
St. Petersburg, Russia	river	May	42.90	19.29	40	29.0
Piermont, USA	river	Aug	43.97	−72.07	15	19.7
Tilton, USA	river	Aug	43.44	−71.59	20	19.7
Charvak, Uzbekistan	river	May	41.62	69.95	35	24.4
Edmonton, Canada	snow	Dec–Jan	53.5	−113.5	39.5	17.2
Triel, France	river	Oct	48.98	2.00	22	16.6

CPD
8, 5493–5543, 2012

Table 2. Precipitation ^{17}O-excess simulated by LMDZ, compared to various additional measurements done at LSCE.

location	sample type	month	lat	lon	reference	^{17}O-excess obs (permeg)	^{17}O-excess LMDZ (permeg)
Zongo, Bolivia	rain	Jun–Aug	−16.15	−67.10	Vimeux et al. (2005), unpublished data	15.7	21.4
Zongo, Bolivia	rain	Dec–Feb	−16.15	−67.10	Vimeux et al. (2005), unpublished data	38.	21.
Niamey, Niger	rain	Jun–15 Jul	13.52	2.09	Risi et al. (2008b); Landais et al. (2010)	−10	8
Niamey, Niger	rain	15 Jul–Oct	13.52	2.09	Risi et al. (2008b); Landais et al. (2010)	20	15
Dome F, Antarctica	snow	annual	−77.32	39.70	Luz and Barkan (2010)	1	10.1
Vostok, Antarctica	snow	annual	−78.45	106.85	Landais et al. (2008)	3.5	−29.9
Vostok, Antarctica	snow	Dec–Feb	−78.45	106.85	Winkler et al. (2012b)	18.5	−11.8
Vostok, Antarctica	snow	Jun–Aug	−78.45	106.85	Winkler et al. (2012b)	−6.4	−33.2
NEEM, Greenland	snow	annual	77.5	−50.9	Landais et al. (2012b)	50	11.1
NEEM, Greenland	snow	Dec–Feb	77.5	−50.9	Landais et al. (2012b)	58.1	29.2
NEEM, Greenland	snow	Jun–Aug	77.5	−50.9	Landais et al. (2012b)	64.9	0.6
Dome C	snow	annual	−75.4	123.14	Winkler et al. (2012b)	18	−9
Taylor	snow	annual	−77.28	158.26	Winkler et al. (2012b)	8.9	4.1
Antarctica transect	snow	annual	−75.6 to −74.4	124.4 to 160.7	Landais et al. (2008)	30 to 59	−22 to −14

CPD
8, 5493–5543, 2012

Table 3. LGM minus present-day difference in precipitation $\delta^{18}O$, d-excess and ^{17}O-excess in Antarctica observed in ice cores and simulated by LMDZ.

	latitude	longitude	$\delta^{18}O$ obs (‰)	d-excess obs (‰)	^{17}O-excess obs (permeg)	$\delta^{18}O$ LMDZ (‰)	d-excess LMDZ (‰)	^{17}O-excess LMDZ (permeg)	reference
Vostok	−78.45	106.85	−14	−1	−20	−8	−1.4	−7	Vimeux et al. (2001a); Landais et al. (2008)
Dome C	−75.4	123.14	−6.5	−2.5	−13	−5.4	−2.6	−35	Stenni et al. (2004), unpublished data
Taylos Dome	−77.28	158.26	−6.7	−6.6	2	−3.5	−4.6	−48	Stenni et al. (2004); Winkler et al. (2012b)
Law Dome	−66.77	112.8	−7	–	4	−3.8	−1.3	−6.7	unpublished data
EDML	−75.0	0.07	−6	−2.5	−2	−4.2	−2.6	−7.3	Stenni et al. (2004); Winkler et al. (2012b)

CPD
8, 5493–5543, 2012

Table 4. Slopes of d-excess and ^{17}O-excess as a function of rh_s. For the data, the slopes correspond to the regression lines shown in red in Fig. 1e, f. For LMDZ and the for the Merlivat and Jouzel (1979) closure equation, the "total" slope correspond to the regression lines shown in blue and green in Fig. 1e, f. The "rh_s effect" is calculated by the difference between the "total" slope and the slope that we would optain if rh_s was set to 60 % everywhere (RH_scste simulation for LMDZ). The "SST effect" is calculated by the difference between the slope that we would optain if rh_s was set to 60 % everywhere, and the slope that we would optain if rh_s was set to 60 % everywhere and if SST was set to 15 °C everywhere (RH_sSSTcste simulation for LMDZ).

data/model	total/rh_s effect/SST effect	d-excess vs rh_s	^{17}O-excess vs rh_s
data	total	−0.60	−0.60
closure	total	−0.58	−0.91
equation	rh_s effect	−0.16	−0.04
	SST effect	−0.43	−0.87
LMDZ	total	−0.22	−0.17
	rh_s effect	−0.15	−0.07
	SST effect	−0.06	0.01

CPD
8, 5493–5543, 2012

Table 5. Summary of the main processes explaining the main features of the $\delta^{18}O$, d-excess and ^{17}O-excess spatio-temporal distribution in the LMDZ model, as a function of latitude.

isotopic tracer		$\delta^{18}O$	d-excess	^{17}O-excess
tropics	latitudinal gradient	re-evaporation	re-evaporation	re-evaporation
	seasonal variation	re-evaporation + convection	re-evaporation + convection	convection + re-evaporation
	LGM–PD difference	ocean composition	re-evaporation	re-evaporation
mid-latitudes	latitudinal gradient	distillation	SST + rh_s	distillation/mixing
	seasonal variation	distillation	RH + condensation conditions	distillation/mixing
	LGM–PD difference	distillation	condensation conditions	distillation/mixing
high latitudes	latitudinal gradient	distillation	distillation + supersaturation	distillation/mixing + supersaturation
	seasonal variation	distillation + rh_s	rh_s + distillation + supersaturation	distillation/mixing + supersaturation
	LGM–PD difference	distillation	distillation + supersaturation	distillation/mixing + supersaturation

CPD
8, 5493–5543, 2012

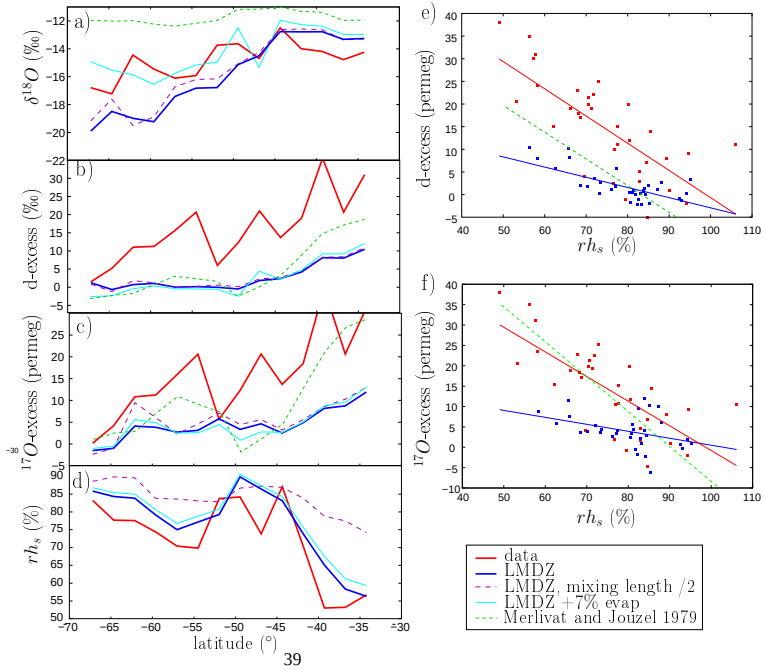

Fig. 1. δ^{18}O **(a)**, d-excess **(b)**, ^{17}O-excess **(c)** and rh_s **(d)** of surface water vapor measured by Uemura et al. (2008, 2010) and simulated by LMDZ, as a function of latitude. Results are regridded on the LMDZ grid and applied a smoothing gaussian filter of 10° in latitude. d-excess **(e)** and ^{17}O-excess **(f)** of surface water vapor measured by Uemura et al. (2008, 2010) and simulated by LMDZ, as a function of surface relative humidity rh_s. Model outputs were collocated with the measurements. Regression coefficients for both simulated and observed values are indicated in table 4. For comparison, the d-excess and ^{17}O-excess of surface water vapor predicted by the Merlivat and Jouzel (1979) closure approximation (Appendix A) is also shown in green. For clarity, we show only the regression line.

CPD
8, 5493–5543, 2012

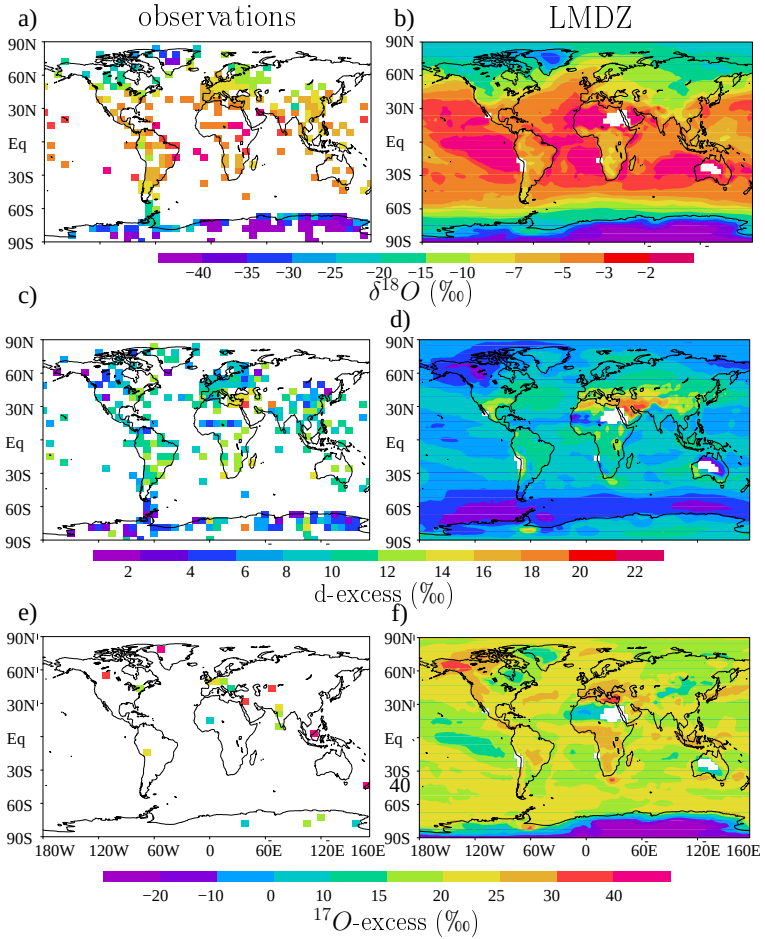

Fig. 2. Annual mean of precipitation δ^{18}O, d-excess and ^{17}O-excess simulated by LMDZ and observed by the GNIP network and various observations listed in Tables 1 and 2.

CPD
8, 5493–5543, 2012

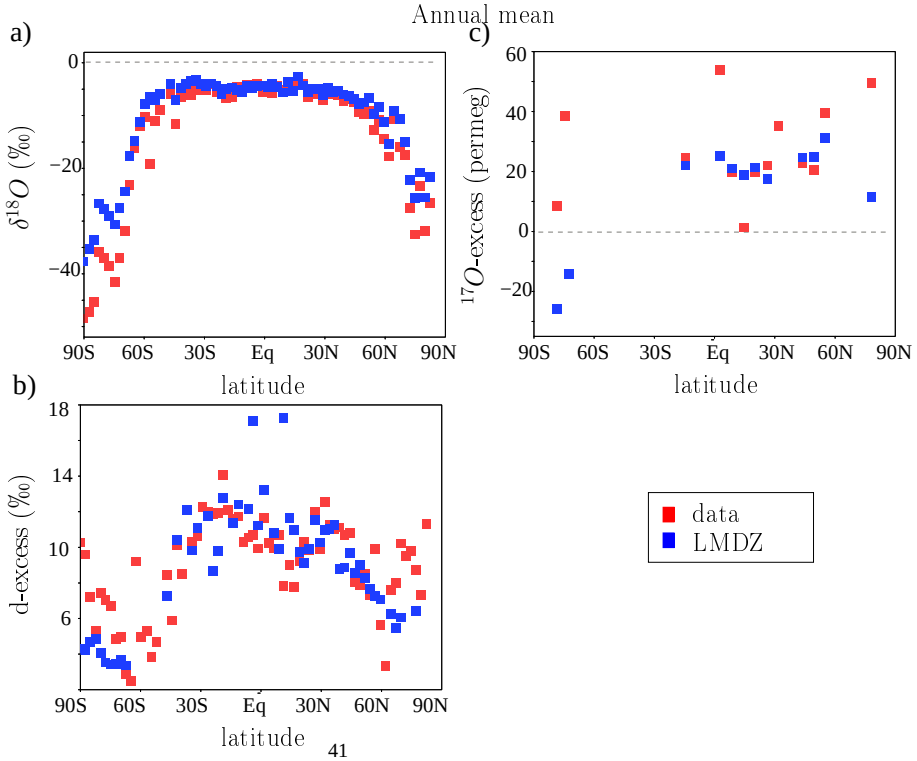

Fig. 3. Annual, zonal mean of precipitation δ^{18}O, d-excess and ^{17}O-excess simulated by LMDZ, compared to the GNIP database for δ^{18}O and d-excess and to the data listed in Tables 1 and 2 for ^{17}O-excess. The model outputs are collocated with the location and month of each measurement.

CPD
8, 5493–5543, 2012

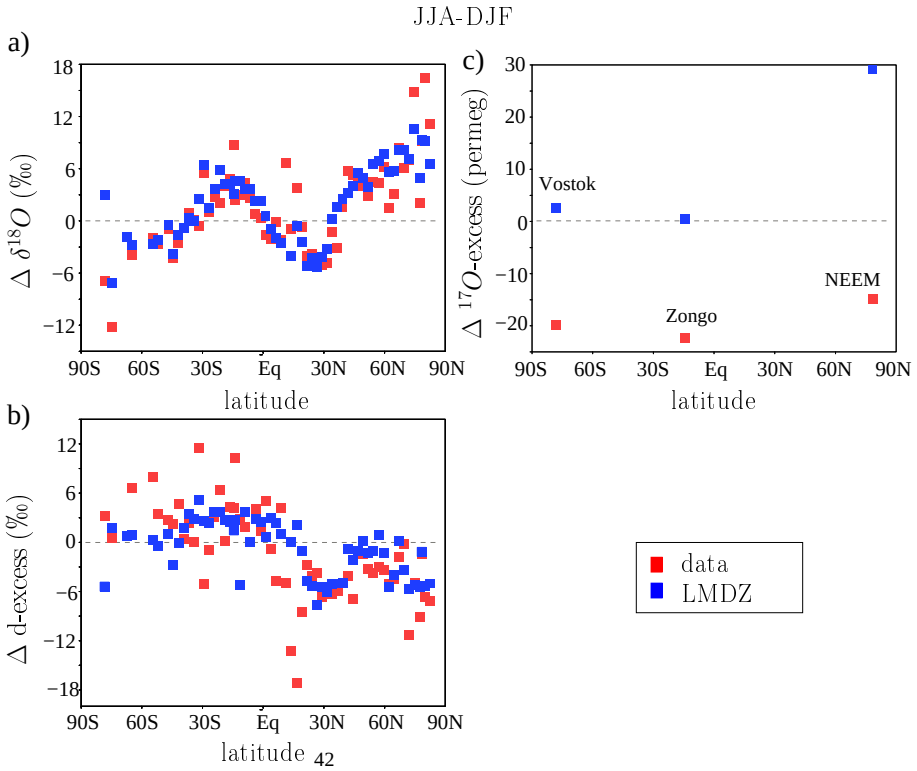

Fig. 4. Same as 3 but for JJA-DJF variations.

CPD
8, 5493–5543, 2012

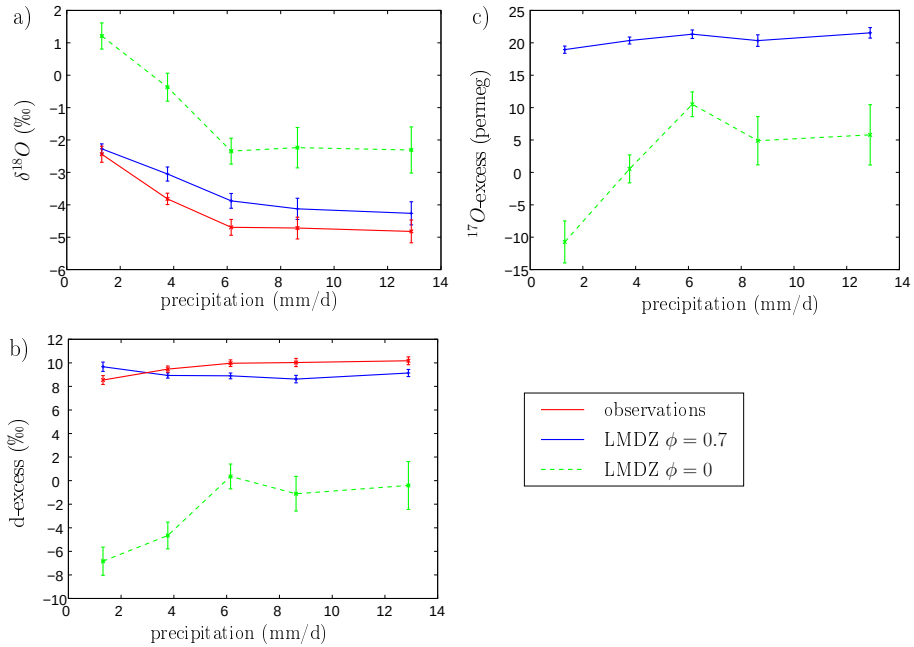

Fig. 5. Composites of precipitation δ^{18}O, d-excess and ^{17}O-excess as a function of precipitation, in the control simulation of LMDZ, in a test in which $\phi = 0$, and in observations. Precipitation range was divided into 6 bins for the composites. Error bars represent the standard deviation within each bin divided by the square root of the number of sample in the bin. LMDZ outputs were collocated with the GNIP observations they are compared wilth. All GNIP observations in oceanic or coastal stations (altitude lower than 20 m) in the tropics (equatorward of 30°) are used. No ^{17}O-excess data are shown due to the lack of data.

CPD
8, 5493–5543, 2012

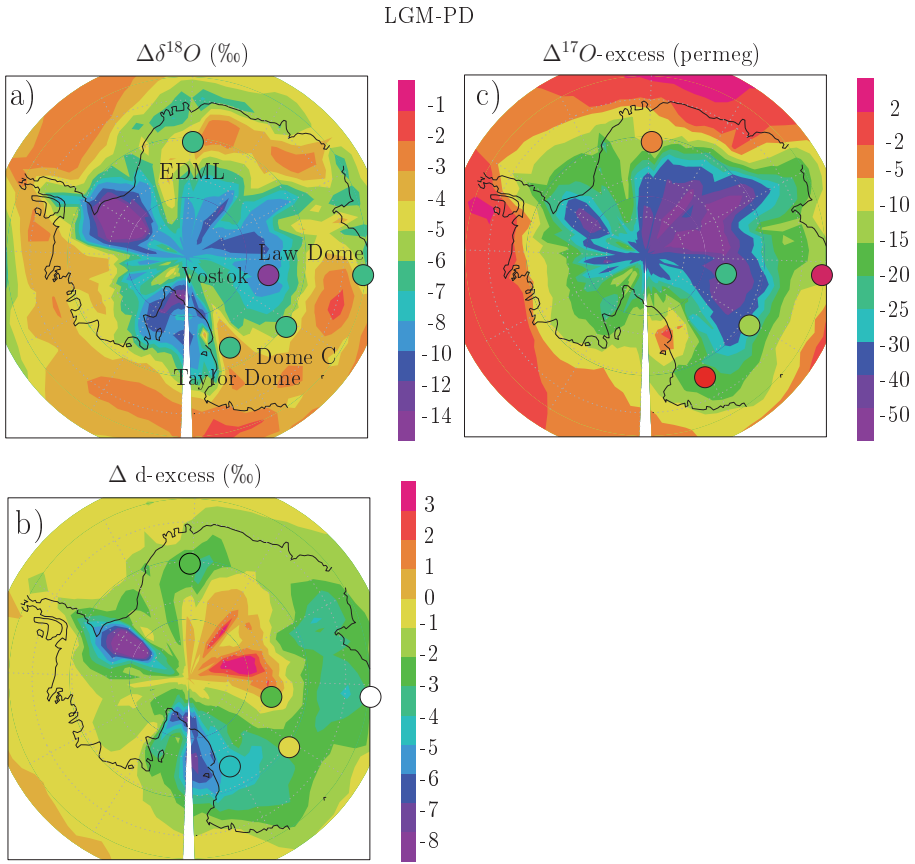

Fig. 6. LGM minus present-day difference in precipitation δ^{18}O, d-excess and ^{17}O-excess in Antarctica observed in ice cores (colored circles) and simulated (shaded) by LMDZ over Antarctica. Numerical values are given in Table 3.

CPD
8, 5493–5543, 2012

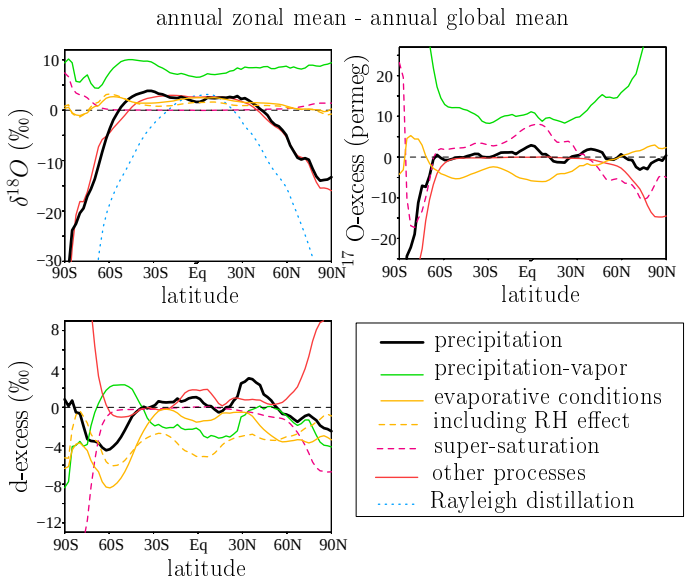

Fig. 7. Decomposition of the annual zonal mean distribution of the precipitation δ^{18}O, d-excess and ^{17}O-excess into different contributions. The black line correspond to the total simulated values. The green, orange, dashed pink and red correspond to the precipitation-vapor difference, the effect of evaporative conditions (SST and rh_s), the effect of supersaturation and all other effects respectively. Their sum makes the total black line. The effect of evaporative conditions is further decomposed into the effect of rh_s only (dashed orange). The difference between the solid and dashed orange lines correspond to the effect of SST only. To focus on spatial patterns, we subtract the annual, global mean to all curves. When the black curve is positive, δ^{18}O, d-excess or ^{17}O-excess are higher than the global mean. When the colored curves are positive, the corresponding process contributes to increase the total values. When the colored curves show a similar shape as the black curve, they contribute to the latitudinal variations of the total signal.

CPD
8, 5493–5543, 2012

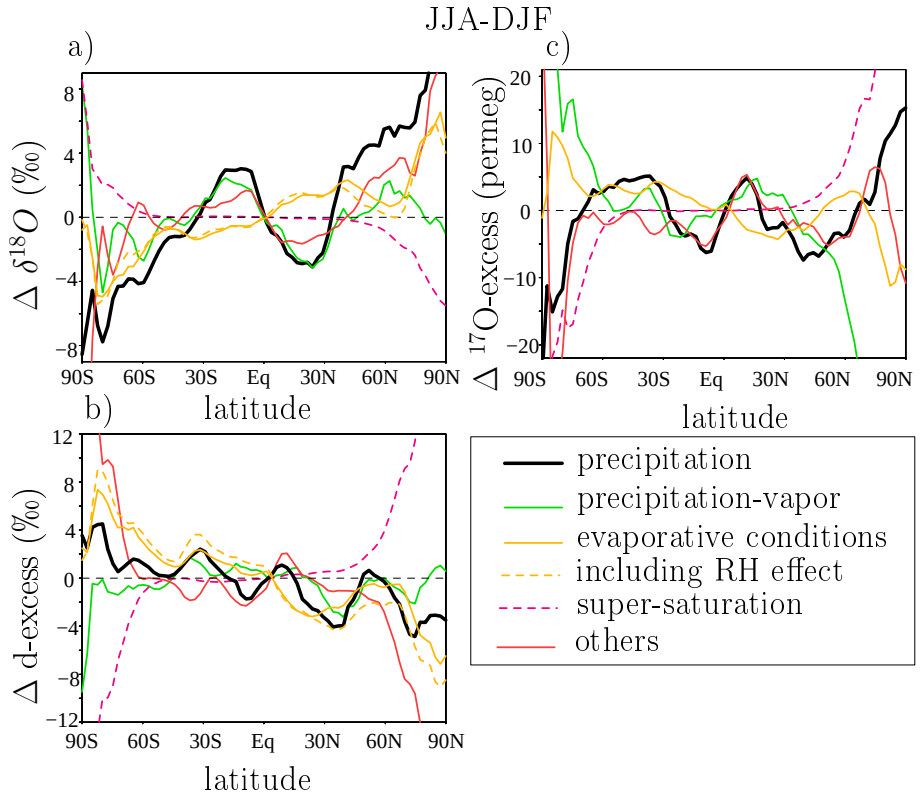

Fig. 8. Same as Fig. 7, but for JJA–DJF differences. When the black line is positive, the δ^{18}O, d-excess or ^{17}O-excess values are higher in JJA than in DJF (i.e. higher in summer in the Northen Hemisphere, higher in winter in the Southern Hemisphere, higher during the wet season in the northen tropics, higher during the dry season in the southern tropics). When the colored curves are of the same sign as the black curves, then the corresponding process contributes positively to the total seasonal signal.

CPD
8, 5493–5543, 2012

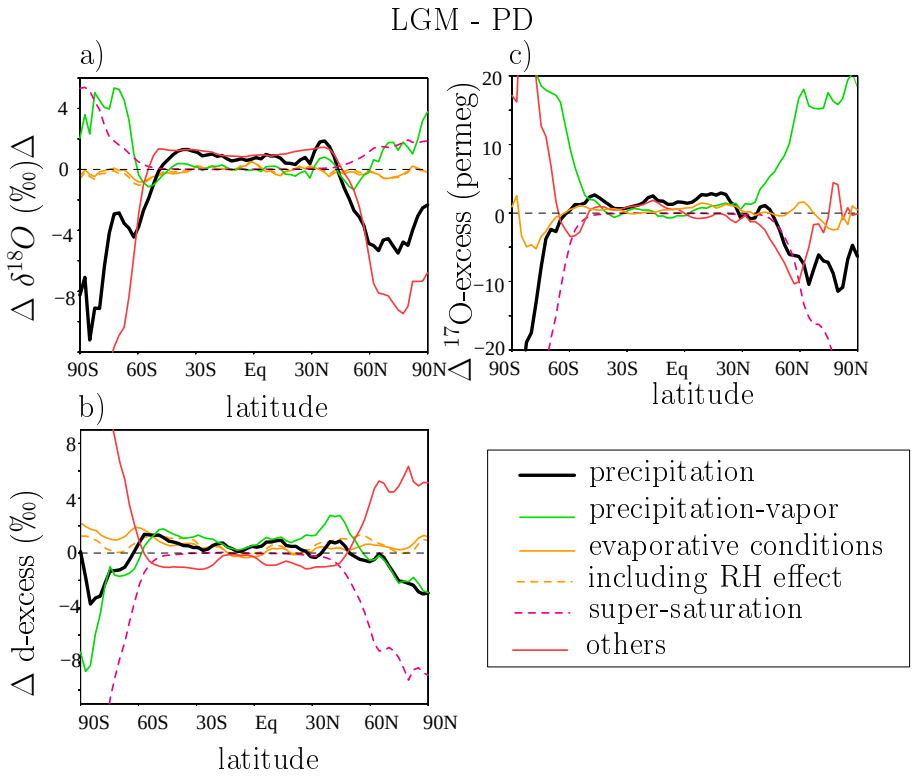

Fig. 9. Same as Fig. 7, but for LGM-PD difference. When the black line is positive, the δ^{18}O, d-excess or ^{17}O-excess values are higher in LGM than in PD. When the colored curves are of the same sign as the black curves, then the corresponding process contributes positively to the total LGM-PD signal.

CPD
8, 5493–5543, 2012

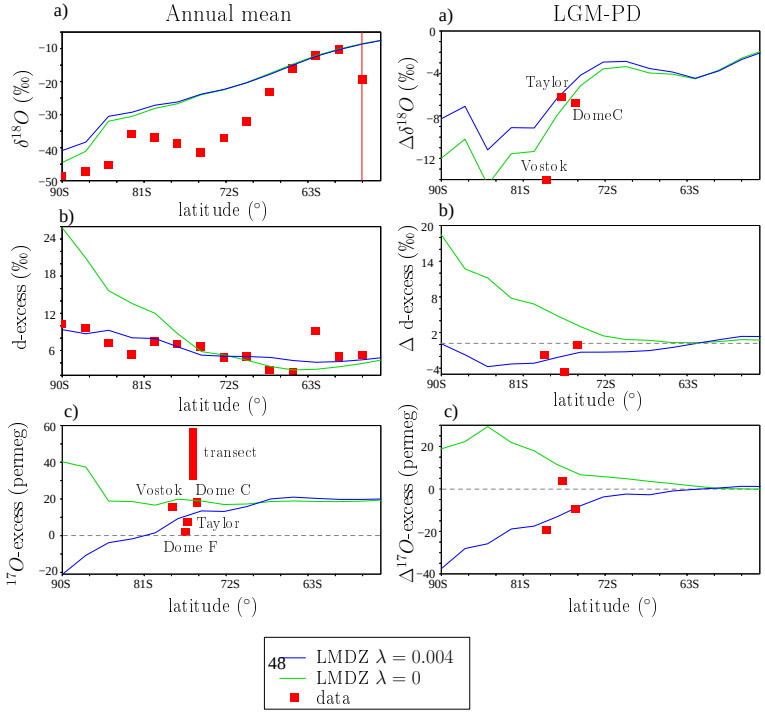

Fig. 10. (a–c) Zonal, annual mean δ^{18}O, d-excess and ^{17}O-excess in precipitation in Antarctica simulated by LMDZ for the control value of λ (blue) and when λ is set to 0 (green). Model outputs are collocated with observations. **(d–f)** Same for zonal, annual mean LGM-PD difference. In all plots, model outputs are compared qualitatively (i.e. with no collocation) with observations (black squares). For δ^{18}O and d-excess, values are zonal averages from the GNIP-Antarctica dataset regridded on LMDZ grid. For ^{17}O-excess, numerical values are those given in Tables 2 and 3.

CPD
8, 5493–5543, 2012